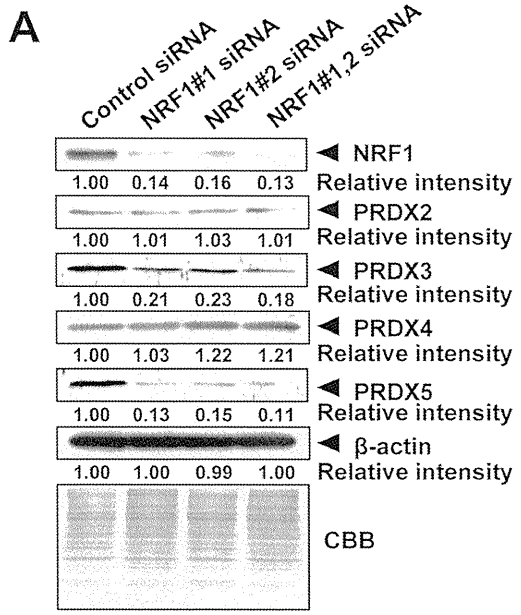

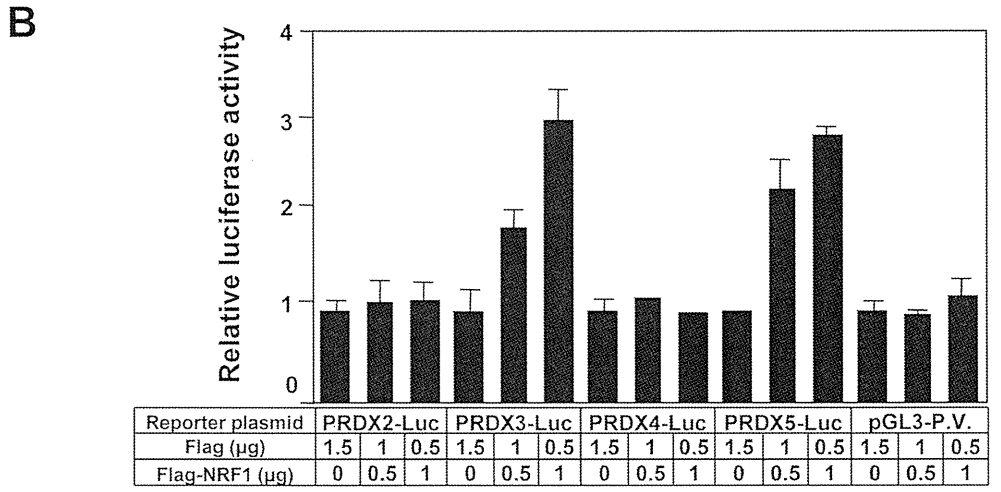

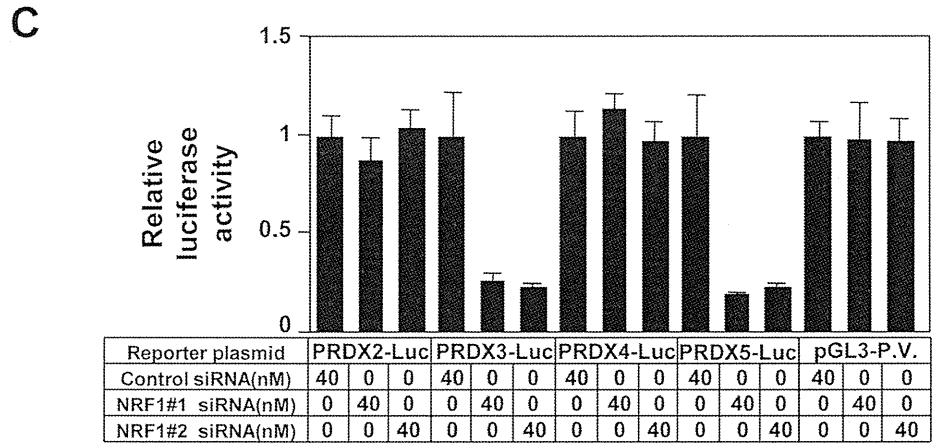

FIGURE 4. (**A**) NRF1 regulates *PRDX3* and *PRDX5* gene expression. Control siRNA (100 pmol) or *NRF1#1* and *#2* siRNA (100 pmol) were transfected into NTM5 cells. Whole nuclear lysates (100 μg for NRF1) and whole cell lysates (50 μg for PRDXs) were subjected to SDS-PAGE. The transferred membrane was blotted with the indicated antibodies. Immunoblotting of β-actin is shown as a loading control. Relative intensity is shown under each blot. CBB, Coomassie brilliant blue. (**B**) NRF1 transactivates the promoter activity of the *PRDX3* and *PRDX5* genes. The indicated amount of NRF1 expression plasmid was transiently cotransfected with the indicated reporter plasmids into NTM5 cells. pGL3-P.V indicates the pGL3 promoter vector in which the luciferase gene is driven by the SV-40 promoter. Results were normalized to protein concentrations measured using the Bradford method. All values are representative of at least three independent experiments. The luciferase activity of each PRDX-Luc construct with transfection of the Flag vector corresponds to 1. Bars represent the SD. (**C**) Knockdown of *NRF1* downregulates the promoter activity of the *PRDX3* and *PRDX5* genes. NTM5 cells were transiently transfected with the indicated amounts of control siRNA or *NRF1* siRNA, followed by transfection with 0.5 μg of the indicated reporter plasmids at intervals of 12 hours. The results shown are normalized to protein concentrations measured using the Bradford method and are representative of at least three independent experiments. The luciferase activity of each PRDX-Luc construct with transfection of control siRNA corresponds to 1. Bars represent the SD.

Quercetin Induces NRF1 Expression through Nrf2 Activation

It has been shown that Nrf2 regulates NRF1 expression.[32] Nrf2 is a cytoplasmic protein translocated to the nuclei by oxidative stress.[33] We therefore examined whether quercetin can increase nuclear Nrf2 expression. As expected, quercetin did induce Nrf2 expression in both a time- and dose-dependent manner (Fig. 5A). Furthermore, we investigated whether the Nrf2 transcription factor can regulate the expression of NRF1 under quercetin treatment. We confirmed that quercetin-dependent induction of NRF1 was completely abolished by the transfection of *Nrf2*-specific siRNA (Fig. 5B). As a control, the expression of Foxo3a and PCNA was not affected by the transfection of siRNA under quercetin

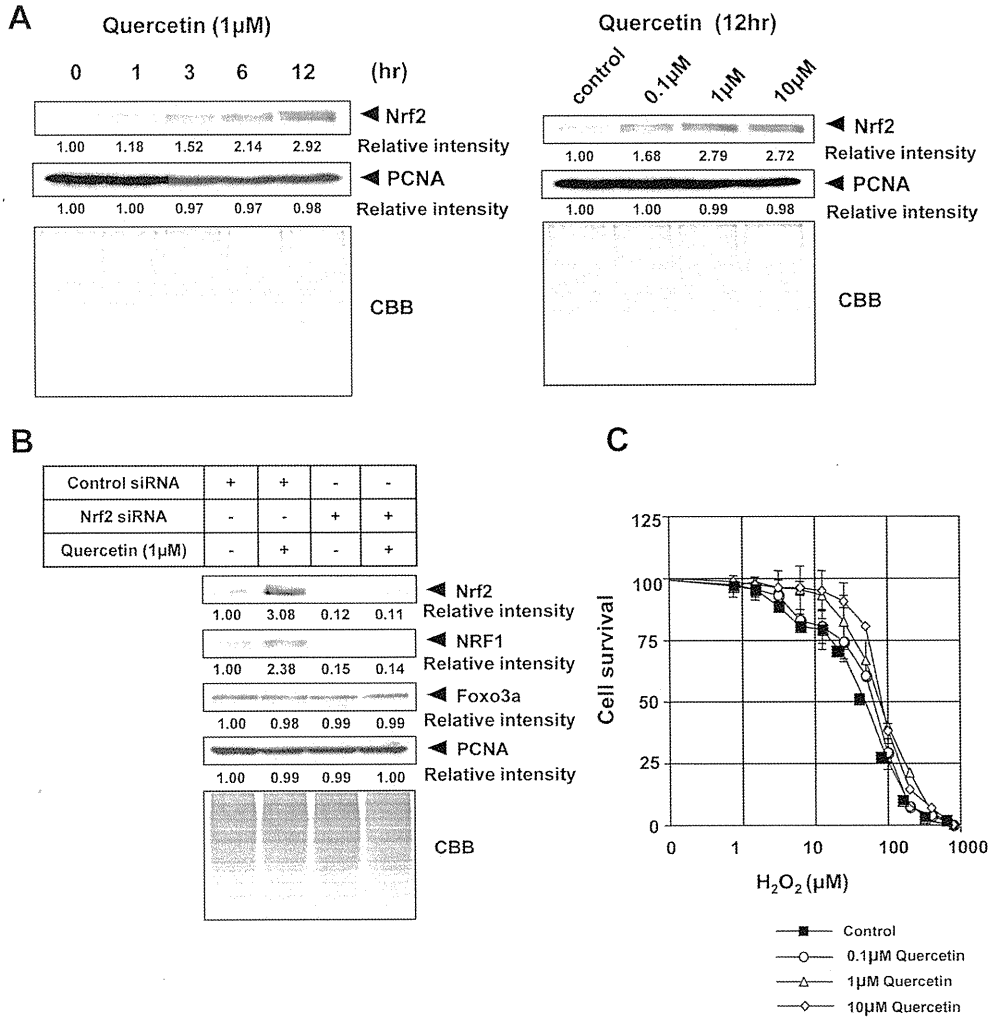

FIGURE 5. (A) Effect of quercetin on expression of Nrf2. *Left*: NTM5 cells were incubated with 1 μM quercetin for the times indicated. Whole nuclear lysates (100 μg) were subjected to SDS-PAGE, and Western blot analysis was performed with the indicated antibodies. Immunoblotting of PCNA is shown as a loading control. Relative intensity is shown under each blot. *Right*: NTM5 cells were cultured for 12 hours in the control medium or in medium containing the indicated concentrations of quercetin. Whole nuclear lysates (100 μg) were subjected to SDS-PAGE, and Western blot analysis was performed with the indicated antibodies. Immunoblotting of PCNA is shown as a loading control. Relative intensity is shown under each blot. (B) NTM5 cells were transiently transfected with 100 pmol control or *Nrf2* siRNAs. The following day, NTM5 cells were cultured in the control medium or in medium containing 1 μM quercetin. After 48 hours, whole nuclear lysates (100 μg) were subjected to SDS-PAGE, and Western blot analysis was performed using the indicated antibodies. Immunoblotting of PCNA is shown as a loading control. Relative intensity is shown at the bottom of the panel. (C) Quercetin treatment counteracts H_2O_2 sensitivity in TM cells. Approximately 2.5×10^3 NTM5 cells were cultured in the control medium or in medium containing the indicated concentration of quercetin. The following day, to induce oxidative stress, cells were incubated with the indicated concentration of H_2O_2 in serum-free medium for 40 minutes After 48 hours, cell survival was analyzed using a WST-8 assay. All values are the means of at least three independent experiments. Bars represent the SD. CBB, Coomassie brilliant blue.

treatment. To examine the protective efficacy of quercetin treatment, TM cells were exposed to H_2O_2 in the presence of quercetin. Quercetin treatment significantly protected the TM cells against the cytotoxic activity of H_2O_2 (Fig. 5C).

NRF1 Expression Modulates Cellular Sensitivity to H_2O_2

PRDX3 localizes to mitochondria and may protect mitochondrial DNA from ROS. NRF1 expression leads to the activation of genes concerned with mitochondrial biogenesis and protects cells from apoptosis.[34] As shown in Figure 6A, the downregulation of PRDX3 and PRDX5 sensitized TM cells approximately twofold against H_2O_2. On the other hand, the downregulation of NRF1 sensitized TM cells approximately fivefold against H_2O_2 (Fig. 6B). Among NRF1-regulated genes, mtTFA is important in protecting mitochondrial DNA from ROS-dependent apoptosis.[35] We showed that quercetin significantly induces mtTFA protein expression (Fig. 6C).

DISCUSSION

Quercetin has a wide variety of pharmacologic properties.[36–40] However, little is known about the mechanisms by which quercetin protects cells against oxidative stress. In the present study, we demonstrated that quercetin stimulates the antioxidant system through the activation of the Nrf2/NRF1 transcription pathway (Figs. 1–4). Quercetin is also a potent free radical scavenger, suggesting that quercetin would be an effective agent against oxidative stress-induced ocular diseases, including glaucoma.

Several transcription factors are activated under oxidative stress induced by hydrogen peroxide and inflammatory cytokines, such as TNF-α and IL-1β. Among them, both NF-κB and Nrf2 are well-known transcription factors related to oxidative stress.[33,41] PRDXs can eliminate hydrogen peroxide efficiently and can participate in many physiological processes such as signal transduction and apoptosis.[42] There are six distinct members located in various subcellular compartments. PRDX1, PRDX2, and PRDX6 are in the cytoplasm, and PRDX3 is found in mitochondria. PRDX4 is in endoplasmic reticulum and is secreted. PRDX5 is found in various compartments. As shown in Figure 1C, the expression of five PRDXs was observed, and both PRDX3 and PRDX5 were induced by the treatment with quercetin in primary TM cells. We have previously shown that PRDX1 is not found in immortalized TM cells.[24] This might be due to the epigenetic mechanism because cellular transformation often induces epigenetic changes such as DNA methylation.[43] We have previously shown that oxidative stress induces *PRDX1* and *PRDX5* through the activation of Ets1.[23] Furthermore, *PRDX2* expression is regulated by the transcription factor Foxo3a.[24] In this study, we found that the Nrf2/NRF1 transcription pathway is also involved in the expression

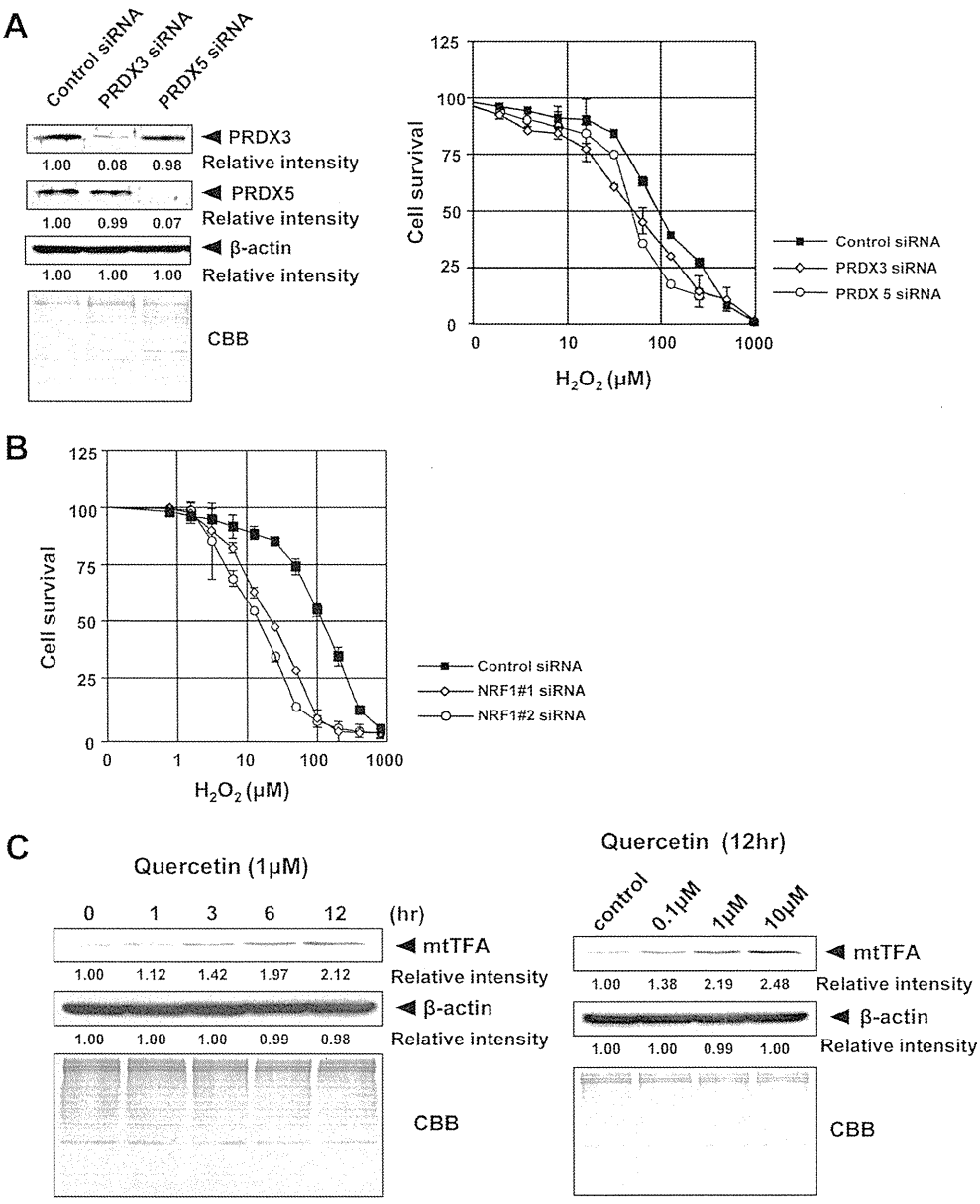

FIGURE 6. (A) Downregulation of *PRDX3* and *PRDX5* sensitizes TM cells to oxidative stress. *Left*: NTM5 cells were transiently transfected with 100 pmol control, *PRDX2,* or *PRDX5* siRNA. After 72 hours, whole cell lysates (50 μg) were subjected to SDS-PAGE, and Western blot analysis was performed using the indicated antibodies. Immunoblotting of β-actin is shown as a loading control. Relative intensity is shown at the bottom of the panel. *Right*: approximately 2.5 × 10^3 NTM5 cells were transfected with 40 nM control siRNA (*filled squares*), *PRDX3* siRNA (*open rhomboids*), or *PRDX5* siRNA (*open circles*). Induction of the indicated concentrations of H_2O_2 was described for Figure 5C. All values are the means of at least three independent experiments. Bars represent the SD. (B) Downregulation of NRF1 sensitizes TM cells to oxidative stress. Approximately 2.5 × 10^3 NTM5 cells were transfected with 40 nM control siRNA (*filled squares*), *NRF1#1* siRNA (*open rhomboids*), or *NRF1#2* siRNA (*open circles*). Induction of the indicated concentrations of H_2O_2 was described for Figure 5C. All values are the means of at least three independent experiments. Bars represent the SD. (C) Effect of quercetin on the expression of mtTFA. *Left*: NTM5 cells were incubated with 1 μM quercetin for the times indicated. Whole cell lysates (100 μg) were subjected to SDS-PAGE, and Western blot analysis was performed with the indicated antibodies. Immunoblotting of β-actin is shown as a loading control. Relative intensity is shown under each blot. *Right*: NTM5 cells were cultured for 12 hours in the control medium or in medium containing the indicated concentration of quercetin. Whole cell lysates (100 μg) were subjected to SDS-PAGE, and Western blot analysis was performed with the indicated antibodies. Immunoblotting of β-actin is shown as a loading control. Relative intensity is shown under each blot. CBB, Coomassie brilliant blue.

of both the *PRDX3* and *PRDX5* genes (Figs. 4, 5). Nrf2, a basic leucine zipper transcription factor, is essential for the inducible and constitutive expression of several phase 2 detoxification proteins, including those required for mitochondrial respiratory function.[44,45] NRF1 was found to act on many nuclear genes required for mitochondrial respiratory function.[46] This primary function was confirmed by disrupting the *Nrf1* gene in mice, resulting in a phenotype of peri-implantation lethality and a striking decrease in the mitochondrial DNA content of Nrf1-null blastocysts.[34]

One specific ROS, hydrogen peroxide, is produced by mitochondria. Because PRDXs can eliminate hydrogen peroxide efficiently, mitochondrial PRDX3 may protect mitochondrial DNA from ROS.[47–50] We have previously reported that a member of the high-mobility group protein family mtTFA can recognize oxidatively damaged DNA.[51,52] Furthermore, it has been shown that mtTFA binds to mitochondrial DNA (mtDNA) in the same way that histones bind to nuclear DNA.[53,54] Because mtTFA is not wrapped by chromatin proteins such as histones, it is highly sensitive to oxidative stress. mtTFA may protect mtDNA, acting as a guardian of mitochondrial function.[55,56] As shown in Figure 6C, quercetin induced mtTFA protein expression. This indicates that quercetin may protect mitochondria from oxidative stress through the induction of both mtTFA and PRDX3. We also demonstrated the protective activity of quercetin against H_2O_2 toxicity (Fig. 5C). Quercetin inhibits the activation of caspase 3 and abolishes the H_2O_2-dependent induction of apoptogenic proteins such as Bcl2.[57] This also suggests that quercetin inhibits the mitochondrial apoptotic pathway induced by various stresses.

The endothelium plays a key role in the maintenance of anterior chamber homeostasis and also is involved in glaucoma pathogenesis.[58] Expression of the PRDX family was investigated in Fuchs' endothelial dystrophy, and the expression of PRDX2, PRDX3, and PRDX5 was significantly downregulated in this disease.[59] It has been reported that PRDX3 oxidation is found in TNF-α–treated cells and is the early event in apoptosis. This leads to an increase of hydrogen peroxide to modulate the progression of apoptosis.[60] These data indicate that the expression of PRDXs in endothelial cells may be also related to

glaucoma pathogenesis. PRDX6 reduces oxidative stress- and TGF-β-induced abnormalities of TM cells.[61] TGF-β is a fibrogenic cytokine and increases ROS production,[62] indicating that our study may be relevant to the physiology and pathophysiology of the outflow pathway in glaucoma.

To our knowledge, this is the first study showing modulation of an oxidative stress-protective pathway involving the control of *PRDX3*, *PRDX5*, and *mtTFA* expression by the transcription factors Nrf2 and NRF1.

References

1. Kook D, Wolf AH, Yu AL, et al. The protective effect of quercetin against oxidative stress in the human RPE in vitro. *Invest Ophthalmol Vis Sci.* 2008;49:1712–1720.
2. Hanneken A, Lin FF, Johnson J, Maher P. Flavonoids protect human retinal pigment epithelial cells from oxidative stress-induced death. *Invest Ophthalmol Vis Sci.* 2006;47:3164–3177.
3. Maher P, Hanneken A. Flavonoids protect retinal ganglion cells from oxidative stress-induced death. *Invest Ophthalmol Vis Sci.* 2005;46:4796–4803.
4. Chow JM, Shen SC, Huan SK, Lin HY, Chen YC. Quercetin, but not rutin and quercitrin, prevention of H_2O_2-induced apoptosis via anti-oxidant activity and heme oxygenase 1 gene expression in macrophages. *Biochem Pharmacol.* 2005;69:1839–1851.
5. Pawlikowska-Pawlega B, Guszecki WI, Misiak LE, Gawron A. The study of the quercetin action on human erythrocyte membranes. *Biochem Pharmacol.* 2003;66:605–612.
6. Johnson JL, Maher PA, Hanneken AM. The flavonoid, eriodictyol, induces long-term protection in ARPE-19 cells through its effects on Nrf2 activation and phase II gene expression. *Invest Ophthalmol Vis Sci.* 2009;50:2398–2406.
7. Saccà SC, Izzotti A, Rossi P, Traverso C. Glaucomatous outflow pathway and oxidative stress. *Exp Eye Res.* 2007;84:389–399.
8. Quigley HA. Number of people with glaucoma worldwide. *Br J Ophthalmol.* 1996;80:389–393.
9. Gordon MO, Beiser JA, Brandt JD, et al. The Ocular Hypertension Treatment Study: baseline factors that predict the onset of primary open-angle glaucoma. *Arch Ophthalmol.* 2002;120:714–720.
10. The Advanced Glaucoma Intervention Study (AGIS), 7: the relationship between control of intraocular pressure and visual field deterioration. The AGIS Investigators. *Am J Ophthalmol.* 2000; 130:429–440.
11. Leske MC, Heijl A, Hussein M, et al. Factors for glaucoma progression and effect of treatment: the early manifest glaucoma trial. *Arch Ophthalmol.* 2003;121:48–56.
12. Feiner L, Piltz-Seymour JR. Collaborative Initial Glaucoma treatment Study. Collaborative Initial Glaucoma Study: a summary of results to data. *Curr Opin Ophthalmol.* 2003;14:106–111.
13. Lutjen-Drecoll E. Functional morphology of the trabecular meshwork in primate eyes. *Prog Retin Eye Res.* 1999;18:91–119.
14. Zhou L, Li Y, Yue BY. Oxidative stress affects cytoskeletal structure and cell-matrix interactions in cells from an ocular tissue: the trabecular meshwork. *J Cell Physiol.* 1999;180:182–189.
15. Maher P, Hanneken A. The molecular basis of oxidative stress-induced cell death in an immortalized retinal ganglion cell line. *Invest Ophthalmol Vis Sci.* 2005;46:749–757.
16. Izzotti A, Bagnis A, Sacca SC. The role of oxidative stress in glaucoma. *Mutat Res.* 2006;612:105–114.
17. He Y, Leung KW, Zhang YH, et al. Mitochondrial complex I defect induces ROS release and degeneration in trabecular meshwork cells of POAG patients: protection by antioxidants. *Invest Ophthalmol Vis Sci.* 2008;49:1447–1458.
18. Chae H, Robison K, Poole L, et al. Cloning and sequencing of thiol-specific antioxidant from mammalian brain: alkyl hydroperoxide reductase and thiol-specific antioxidant define a large family of antioxidant enzymes. *Proc Natl Acad Sci U S A.* 1994;91:7017–7021.
19. Rhee SG, Kang SW, Chang TS, Jeong W, Kim K. Peroxiredoxin, a novel family of peroxidases. *IUBMB Life.* 2001;52:35–41.
20. Hofmann B, Hecht HJ, Flohé L. Peroxiredoxins. *Biol Chem.* 2002; 383:347–364.
21. Wood ZA, Schröder E, Robin Harris J, Poole LB. Structure, mechanism and regulation of peroxiredoxins. *Trends Biochem Sci.* 2003;28:32–40.
22. Rhee SG, Chae HZ, Kim K. Peroxiredoxins: a historical overview and speculative preview of novel mechanisms and emerging concepts in cell signaling. *Free Radic Biol Med.* 2005;38:1543–1552.
23. Shiota M, Izumi H, Miyamoto N, et al. Ets regulates peroxiredoxin 1 and 5 expressions through their interaction with the high mobility group protein B1. *Cancer Sci.* 2008;99:1950–1959.
24. Miyamoto N, Izumi H, Miyamoto R, et al. Nipradilol and timolol induce forkhead transcription factor Foxo3a and peroxiredoxin 2 expression and protect trabecular meshwork cells from oxidative stress. *Invest Ophthalmol Vis Sci.* 2009;50:2777–2784.
25. Pang IH, Shade DL, Clark AF, Steely HT, DeSantis L. Preliminary characterization of a transformed cell stain derived from human trabecular meshwork. *Curr Eye Res.* 1994;13:51–63.
26. Izumi H, Ohta R, Nagatani G, et al. p300/CBP-associated factor (P/CAF) interacts with nuclear respiratory factor-1 to regulate the UDP-N-acetyl-α-D-galactosamine: polypeptide N- acetylgalactosaminlytransferase-3 gene. *Biochem J.* 2003;373:713–722.
27. Yoshida Y, Izumi H, Ise T, et al. Human mitochondrial transcription factor A binds preferentially to oxidative damaged DNA. *Biochem Biophys Res Commun.* 2002;295:945–951.
28. Araki M, Nanri H, Ejima K, et al. Antioxidant function of the mitochondrial protein SP-22 in the cardiovascular system. *J Biol Chem.* 1999;274:2271–2278.
29. Igarashi T, Izumi H, Uchiumi T, et al. Clock and ATF4 transcription system regulates drug resistance in human cancer cell lines. *Oncogene.* 2007;26:4749–4760.
30. Miyamoto N, Izumi H, Noguchi T, et al. Tip60 is regulated by circadian transcription factor Clock and is involved cisplatin resistance. *J Biol Chem.* 2008;26:18218–18226.
31. Fatma N, Kubo E, Toris CB, et al. PRDX6 attenuates oxidative stress- and TGFbeta-induced abnormalities of human trabecular meshwork cells. *Free Radic Res.* 2009;43:783–795.
32. Piantadosi CA, Carraway MS, Babiker A, Suliman HB. Heme oxygenase-1 regulates cardiac mitochondrial biogenesis via Nrf2-mediated transcriptional control of nuclear respiratory factor-1. *Circ Res.* 2008;103:1232–1240.
33. Nguyen T, Nioi P, Pickett CB. The Nrf2-antioxidant response element signaling pathway and its activation by oxidative stress. *J Biol Chem.* 2009;284:13291–13295.
34. Huo L, Scarpulla RC. Mitochondrial DNA instability and peri-implantation lethality associated with targeted disruption of nuclear respiratory factor 1 in mice. *Mol Cell Biol.* 2001;21:644–654.
35. Piantadosi CA, Suliman HB. Mitochondrial transcription factor A induction by redox activation of nuclear respiratory factor 1. *J Biol Chem.* 2006;281:324–333.
36. Chen YC, Chen SC, Lin YC. Rutinoside at C7 attenuates the apoptosis-including activity of flavonoids. *Biochem Pharmacol.* 2003;66:1139–1150.
37. Ko CH, Shen SC, Chen YC. Hydroxylation at C4′ or C6 is essential for apoptosis-inducing activity of flavanone through activation of the caspase-3 cascade and production of reactive oxygen species. *Free Radic Biol Med.* 2004;36:897–910.
38. Shen SC, Ko CH, Tseng SW, Tsai SH, Chen YC. Structurally related antitumor effects of flavanones in vitro and vivo: involvement of caspase 3 activation, p21 gene expression, and reactive oxygen species production. *Toxicol Appl Pharmacol.* 2004;197:84–95.
39. Shen SC, Ko CH, Hsu KC, Chen YC. 3-OH flavones inhibition of epidermal growth factor-induced proliferation through blocking prostaglandin E2 production. *Int J Cancer.* 2004;108:502–510.
40. Lin HY, Juan SH, Shen SC, Hsu FL, Chen YC. Inhibition of lipopolisaccharide-induced nitric oxide production by flavonoids in RAW 264.7 macrophages involves heme oxygenase-1. *Biochem Pharmacol.* 2003;66:1821–1832.
41. Gloire G, Legrand-Poels S, Piette J. NF-kappaB activation by reactive oxygen species: fifteen years later. *Biochem Pharmacol.* 2006; 72:1493–1505.
42. Oláhová M, Taylor SR, Khazaipoul S, et al. A redox-sensitive peroxiredoxin that is important for longevity has tissue- and stress-specific roles in stress resistance. *Proc Natl Acad Sci U S A.* 2008;105:19839–19844.

43. Ferrari R, Berk AJ, Kurdistani SK. Viral manipulation of the host epigenome for oncogenic transformation. *Nat Rev Genet.* 2009; 10:290–294.
44. Itoh K, Ishii T, Wakabayashi N, Yamamoto M. Regulatory mechanisms of cellular response to oxidative stress. *Free Radic Res.* 1999;31:319–324.
45. Ishii T, Itoh K, Takahashi S, Sato H, et al. Transcription factor Nrf2 coordinately regulates a group of oxidative stress-inducible genes in macrophages. *J Biol Chem.* 2000;275:16023–16029.
46. Scarpulla RC. Transcription activators and coactivators in the nuclear control of mitochondrial function in mammalian cells. *Gene.* 2002;286:81–89.
47. Noh YH, Baek JY, Jeong W, Rhee SG, Chang TS. Sulfiredoxin translocation into mitochondria plays a crucial role in reducing hyperoxidized peroxiredoxin III. *J Biol Chem.* 2009;284:8470–8477.
48. Chang TS, Cho CS, Park S, et al. Peroxiredoxin III, a mitochondrion-specific peroxidase, regulates apoptotic signaling by mitochondria. *J Biol Chem.* 2004;279:41975–41984.
49. Wood ZA, Poole LB, Karplus PA. Peroxiredoxin evolution and the regulation of hydrogen peroxide signaling. *Science.* 2003;300: 650–653.
50. Giorgio M, Trinei M, Migliaccio E, Pelicci PG. Hydrogen peroxide: a metabolic by-product or a common mediator of ageing signals? *Nat Rev Mol Cell Biol.* 2007;8:722–728.
51. Prasad R, Liu Y, Deterding LJ, et al. HMGB1 is a cofactor in mammalian base excision repair. *Mol Cell.* 2007;27:829–841.
52. Yoshida Y, Izumi H, Torigoe T, et al. P53 physically interacts with mitochondrial transcription factor A and differentially regulates binding to damaged DNA. *Cancer Res.* 2003;63:3729–3734.
53. Alam TI, Kanki T, Muta T, et al. Human mitochondrial DNA is packaged with TFAM. *Nucleic Acids Res.* 2003;31:1640–1645.
54. Kanki T, Ohgaki K, Gaspari M, et al. Architectural role of mitochondrial transcription factor A in maintenance of human mitochondrial DNA. *Mol Cell Biol.* 2004;24:9823–9834.
55. Larsson NG, Wang J, Wilhelmsson H, et al. Mitochondrial transcription factor A is necessary for mtDNA maintenance and embryogenesis in mice. *Nat Genet.* 1998;18:231–236.
56. Wang J, Silva JP, Gustafsson CM, Rustin P, Larsson NG. Increased in vivo apoptosis in cells lacking mitochondrial DNA gene expression. *Proc Natl Acad Sci U S A.* 2001;98:4038–4043.
57. Park C, So HS, Shin CH, Baek SH. Quercetin protects the hydrogen peroxide-induced apoptosis via inhibition of mitochondrial dysfunction in H9c2 cardiomyoblast cells. *Biochem Pharmacol.* 2003; 66:1287–1295.
58. Resch H, Garhofer G, Fuchsjäger-Mayrl G, Hommer A, Schmetterer L. Endothelial dysfunction in glaucoma. *Acta Ophthalmol.* 2009; 87:4–12.
59. Jurkunas UV, Rawe I, Bitar MS, et al. Decreased expression of peroxirdoxins in Fuchs' endothelial dystrophy. *Invest Ophthalmol Vis Sci.* 2008;49:2956–2963.
60. Cox AG, Pullar JM, Hughes G, Ledgerwood EC, Hampton MB. Oxidation of mitochondrial peroxiredoxin 3 during the initiation of receptor-mediated apoptosis. *Free Radic Biol Med.* 2008;44: 1001–1009.
61. Liu RM, Gaston Pravia KA. Oxidative stress and glutathione in TGF-beta-mediated fibrogenesis. *Free Radic Biol Med.* 2010;48: 1–15.
62. Liu RM, Choi J, Wu JH, et al. Oxidative modification of nuclear mitogen-activated protein kinase phosphatase 1 is involved in transforming growth factor beta1-induced expression of plasminogen activator inhibitor 1 in fibroblasts. *J Biol Chem.* 2010;285: 16239–16247.

Transcriptional Regulation of Activating Transcription Factor 4 under Oxidative Stress in Retinal Pigment Epithelial ARPE-19/HPV-16 Cells

Naoya Miyamoto,[1,2] *Hiroto Izumi,*[1] *Rie Miyamoto,*[2] *Han Bin,*[1] *Hiroyuki Kondo,*[2] *Akihiko Tawara,*[2] *Yasuyuki Sasaguri,*[3] *and Kimitoshi Kohno*[1]

Purpose. Oxidative stress plays an important role in the pathogenesis of various ocular diseases such as retinopathy, glaucoma, and age-related macular degeneration. Activating transcription factor 4 (ATF4) is induced by various stressors, including endoplasmic reticulum (ER) and oxidative stress, and ATF4 expression is regulated translationally through the PERK pathway of eIF2α phosphorylation. Transcriptional regulation of the *ATF4* gene under oxidative stress was investigated in human papillomavirus 16 (HPV-16)–transformed retinal pigment epithelial ARPE-19/HPV-16 cells.

Methods. Retinal pigment epithelial cells, trabecular meshwork cells, and corneal endothelial cells were treated with anoxia and thapsigargin (TG). Gene expression of ATF4 and nuclear factor (erythroid-derived 2)-like 2 (Nrf2) and transcription factors was investigated by Western blot analysis, reporter assays, chromatin immunoprecipitation (ChIP) assays, and small interfering (si)RNA strategies. Cellular sensitivity to oxidative stress was determined.

Results. The expression of two transcriptional factors, ATF4 and Nrf2, was significantly induced by anoxia and TG. The Nrf2 regulator Keap1 was downregulated by anoxia. Downregulation of Nrf2 abolished ATF4 expression. On the other hand, downregulation of Keap1 enhanced the expression of both Nrf2 and ATF4. The promoter activity of ATF4 was transactivated by the co-transfection of Nrf2 expression plasmids and reduced by the transfection of Nrf2-specific siRNA. The ChIP assays demonstrated that Nrf2 bound to the promoter of the *ATF4* gene. Nrf2 downregulation nearly abolished the ATF4 induction by anoxia and TG. Consistent with these findings, the promoter activity of ATF4 was augmented by treatment with TG, HCA, H_2O_2, and anoxia. However, stress induction of ATF4 promoter activity was observed, even when a mutation was introduced into the antioxidant-responsive elements site. Furthermore, stress induction of the ATF4 promoter was completely abolished when the 5′ untranslated region of the *ATF4* gene was deleted. Downregulation of ATF4 rendered ARPE-19/HPV-16 cells sensitive to oxidative stress.

Conclusions. These results suggest that the stress induction of ATF4 is significantly regulated transcriptionally through a Nrf2-dependent mechanism and may be a double-edged sword in the pathogenesis of various retinopathies. (*Invest Ophthalmol Vis Sci.* 2011;52:1226–1234) DOI:10.1167/iovs.10-5775

The eye is protected against oxidative stress by several mechanisms. We have shown that transcription factor Foxo3a functions to protect trabecular meshwork cells from oxidative stress.[1] We have also reported that activating transcription factor 4 (ATF4) is upregulated in drug-resistant cells and protects against oxidative stress through glutathione biosynthesis.[2,3] Thus, in addition to the transcription factor Foxo3a, the *ATF4* gene is thought to be one of the critical transcriptional factors for a cellular response against oxidative stress.

Cellular stress, including oxidative stress, activates the PERK pathway, and phosphorylation of the translational initiation factor eIF2α subsequently causes ATF4 expression to be translationally activated.[4–6] Phosphorylation of eIF2α leads to a general inhibition of translation[7–10]; however, translation of ATF4 mRNA is selectively processed, the mechanism of which has been elucidated in the general amino acid control response in yeast.[4,11] The translational upregulation of the transcription of the *ATF4* gene remains to be elucidated.

Nuclear factor (erythroid-derived 2)-like 2 (Nrf2) is essential for inducible and constitutive expression of several phase II detoxification enzymes and antioxidant enzymes. During an oxidative stress condition, Nrf2 dissociates with Keap1, which is involved in cytoplasmic sequestration of Nrf2, and translocates into the nucleus, activating target genes by heterodimerizing with the small Maf family and binding to antioxidant-responsive elements (AREs).[12–16] Both Nrf2 and ATF4 are coordinately activated by oxidative stress.[17–19]

In the present study, we showed that Nrf2 is involved in transcriptional *ATF4* gene expression under oxidative stress and that the *ATF4* gene is one of the Nrf2 target genes.

Methods

Cell Culture

The human retinal pigment epithelium cell line ARPE-19/HPV-16 (CRL-2502)[20] and the bovine corneal endothelial cell line BCE C/D-1b (CRL-2048)[21] were obtained from the American Type Culture Collection (Manassas, VA). ARPE-19/HPV-16 cells were cultured in a 1:1 mixture of Dulbecco's modified Eagle's medium and Ham's F12-medium (DMEM: F12). BCE C/D-1b cells and an immortalized TM cell line (i.e., NTM5 cells derived from normal trabecular meshwork),[1,22] were cultured in Dulbecco's modified Eagle's medium. All cell lines were maintained in a 5% CO_2 atmosphere at 37°C. The primary human retinal pigment epithe-

From the Departments of [1]Molecular Biology, [2]Ophthalmology, and [3]Pathology and Cell Biology, School of Medicine, University of Occupational and Environmental Health, Japan, Fukuoka, Japan.

Supported in part by Grants-in-Aid for Scientific Research from the Ministry for Education, Culture, Sports, Science and Technology of Japan (17016075), UOEH Grant for Advanced Research, and The Vehicle Racing Commemorative Foundation.

Submitted for publication April 26, 2010; revised September 13 and October 7 and 18, 2010; accepted October 18, 2010.

Disclosure: **N. Miyamoto**, None; **H. Izumi**, None; **R. Miyamoto**, None; **H. Bin**, None; **H. Kondo**, None; **A. Tawara**, None; **Y. Sasaguri**, None; **K. Kohno**, None

Corresponding author: Kimitoshi Kohno, Department of Molecular Biology, School of Medicine, University of Occupational and Environmental Health, 1-1 Iseigaoka, Yahatanishi-ku, Kitakyushu 807-8555, Japan; k-kohno@med.uoeh-u.ac.jp.

lial cells, HRPEpiC, was purchased from Sciencell Research Laboratories (San Diego, CA). Early passages (3–4) of HRPEpiCs were used in the study.

Antibodies and Drugs

Antibodies against Nrf2 (sc-30915), ATF4 (sc-200), Keap1 (sc-15,246), and PCNA (sc-56) were purchased from Santa Cruz Biotechnology (Santa Cruz, CA). Anti-Nrf2 antibody (RB10471P), anti-β-actin antibody (AC-15), and anti-HA-peroxidase (3F10) were purchased from Thermo Scientific, Inc. (Bremen, Germany), Sigma-Aldrich (St. Louis, MO), and Roche Molecular Biochemicals (Mannheim, Germany), respectively. Thapsigargin (TG) and homocysteine (HCA) were purchased from Sigma-Aldrich. Drug concentrations in this study corresponded with those used in clinical practice.

Plasmid Construction

To obtain full-length complementary (c)DNA for human *Nrf2*, we performed PCR on a cDNA library (SuperScript; Invitrogen Life Technologies, Carlsbad, CA), using the following primer pairs (italic indicates the start and stop codons): 5′-*ATG*ATGGACTTGGAGCTGCCGCC-3′ and 5′-*CTA*GTTTTTCTTAACATCTGGCTTCTTAC-3′. This PCR product was cloned into a vector (pGEM-T Easy; Promega, Madison, WI). To construct a plasmid expressing HA tagged *Nrf2*, N-terminal HA-tagged *Nrf2* cDNA was ligated into a pcDNA3 vector (Invitrogen Life Technologies). The luciferase reporter constructs containing the core promoter and the partial first exon with either the short (−314 to +81) or long (−314 to +877) 5′ untranslated region (UTR) of ATF4 were generated by using the following primers: primer 1, 5′-*AGATCT*GCGCTGACACCGGAAGCGAGGCG-3′; primer 2, 5′-*AGATCT*GCGCGGACACC**AT**AAGCGAGGCG-3′; primer 3, 5′-*AAGCTT*GGCCGTGGACCCTGAGGGC-3′; and primer 4, 5′-*AAGCTT*TGCTGGAATCGAGGAATGTGC-3′. Italic and bold indicate restriction enzyme cleavage sites and mutations of ARE, respectively. To obtain *ATF4*-Luc WS, *ATF4*-Luc WL, *ATF4*-Luc MS, and *ATF4*-Luc ML, PCR using placental DNA was performed with primers 1 and 3, primers 1 and 4, primers 2 and 3, and primers 2 and 4, respectively. These PCR products were cloned and ligated into the *Bgl*II-*Hin*dIII sites of the pGL3-basic vector (Promega).

Knockdown Analysis with siRNAs

The following double-stranded RNA 25-bp oligonucleotides were commercially generated (Invitrogen): *ATF4* small interfering RNA (siRNA), 5′-GGGCAGUGAAGUGGAUAUCACUGAA-3′ (sense) and 5′-UUCAGUGAUAUCCACUUCACUGCCC-3′ (antisense), *ATF4*-1 siRNA; 5′-GGGCUGAAGAAAGCCUAGGUCUCUU-3′ (sense) and 5′-AAGAGACCUAGGCUUUCUUCAGCCC-3′ (antisense), *ATF4*-2 siRNA; 5′-UCACUUUGCAAAGCUUUCAACCAAA-3′ (sense) and 5′-UUUGGUUGAAAGCUUUGCAAAGUGA-3′ (antisense), *Nrf2*-1 siRNA; 5′-GACACACUACUUGGCCUCAGUGAUU-3′ (sense) and 5′-AAUCACUGAGGCCAAGUAGUGUGUC-3′ (antisense), *Nrf2*-2 siRNA; 5′-CCAACCAGUUGACAGUGAACUCAUU-3′ (sense) and 5′-AAUGAGUUCACUGUCAACUGGUUGG-3′ (antisense), *Nrf2*-3 siRNA; 5′-GGAAACAGAGACGUGGACUUUCGUA-3′ (sense) and 5′-UACGAAAGUCCACGUCUCUGUUUCC-3′ (antisense), *Keap1*-1 siRNA; 5′-UCCACGUCAUGAACGGUGCUGUCAU-3′ (sense) and 5′-AUGACAGCACCGUUCAUGACGUGGA-3′ (antisense), *Keap1*-2 siRNA; and 5′-GCCCGGGAGUACAUCUACAUGCAUU-3′ (sense) and 5′-AAUGCAUGUAGAUGUACUCCCGGGC-3′ (antisense), *Keap1*-3 siRNA. siRNA transfections were performed as described previously.[1,3,23] Briefly, 250 picomoles of the indicated siRNAs or control siRNA (Invitrogen) were transfected to 1×10^6 NTM5 cells, 2×10^5 cells were used for the luciferase assay, and 2.5×10^3 cells were used for the WST-8 assay described in the following sections. The remaining cells were subjected to Western blot analysis after 72 hours culture as described below.

Western Blot Analysis

The preparation of whole nuclear extracts is described elsewhere.[3,23] The indicated amounts of whole nuclear extracts were separated by sodium dodecyl sulfate-polyacrylamide gel electrophoresis (SDS-PAGE) and transferred to polyvinylidene difluoride (PVDF) microporous membranes (Millipore, Billerica, MA), by using a semidry blotter. The blotted membranes were treated with 5% (wt/vol) skimmed milk in 10 mM Tris, 150 mM NaCl and 0.2% (vol/vol) Tween 20, and were incubated for 1 hour at room temperature with primary antibody. The following antibodies and dilutions were used: a 1:500 dilution of anti-Nrf2, a 1:1,000 dilution of anti-Keap1, a 1:5,000 dilution of anti-ATF4, a 1:5,000 dilution of anti-PCNA, and a 1:20,000 dilution of anti-β-actin. Membranes were then incubated for 40 minutes at room temperature with a peroxidase-conjugated secondary antibody and were visualized with chemiluminescence (ECL kit; GE Healthcare Bio-Science, Piscataway, NJ). Membranes were then exposed to autoradiograph film (X-OMAT film; Eastman Kodak, Rochester, NY). The reproducibility was confirmed by several Western blot analyses, and the resulting blots are shown in the figures. For the correlation assay, the intensity of each signal was quantified by the NIH Image program (NIH, Bethesda, MD; developed by Wayne Rasband, National Institutes of Health, Bethesda, MD; available at http://rsb.info.nih.gov/ij/index.html).

Luciferase Assay

Transient transfection and a luciferase assay were performed as described elsewhere.[1,3,23] In preparing expression plasmids, 2×10^5 ARPE-19/HPV-16 cells per well were seeded into 12-well plates. The following day, indicated amounts of reporter plasmids (see Figs. 3 and 5) were transfected with or without expression plasmids (Superfect reagent; Qiagen, Valencia, CA). After 48 hours, the luciferase activity was detected with a kit (PicaGene; Toyo Ink, Tokyo, Japan). At 24 hours after transfection with indicated siRNAs described earlier, indicated amounts of reporter plasmids were transfected with the reagent (Superfect; Qiagen). After 48 hours, the luciferase activity was detected using the assay (PicaGene; Toyo Ink). For treatment with TG or HCA, 1 μM TG or 1 mM HCA were directly added into the culture medium at 36 hours after transfection. After 6 hours, the luciferase activity was detected with the kit (PicaGene; Toyo Ink). For H_2O_2 or anoxic treatment conditions, at 42 or 40 hours after transfection, cells were cultured with 500 μM H_2O_2 for 2 hours or under anoxic conditions (Anaerocult A mini; Merck, Darmstadt, Germany) creating oxygen-free circumstances for 4 hours, respectively. Cells treated with H_2O_2 or anoxic conditions and mock treated cells were further cultured with a new normal culture medium and normal conditions for 4 hours by recovery/reoxygenation. The light intensity was measured with a luminometer (Luminescencer JNII RAB-2300; ATTO). The results shown are normalized to the protein concentrations measured using the Bradford method and are representative of at least three independent experiments.

Chromatin Immunoprecipitation Assay

The chromatin immunoprecipitation assay (ChIP) assay was performed as described previously. Briefly, soluble chromatin from ARPE-19/HPV16 cells was incubated with 2 μg anti-Nrf2 antibody (sc-722), anti-Nrf2 antibody (RB10471P), and normal rabbit immunoglobulin G (IgG). Immunoprecipitated DNAs with protein A/G-agarose were purified and dissolved in 20 μL of distilled H_2O. Each 2 μL of DNA was used for PCR analysis with the following primer pairs; ATF4 (−308 to +81), 5′-GCGCTGACACCGGAAGCGAGGCG-3′ (forward) and 5′-GGCCGTGGACCCTGAGGGC-3′ (reverse); YB-1 (+409 to +936), 5′-GCCCGGCACTACGGGCTGCG-3′ (forward) and 5′-GTGTGCGCAGGCCGCGGACG-3′ (reverse). The PCR products were separated by electrophoresis on 2% agarose gels and stained with ethidium bromide.

Cytotoxicity Analysis with WST-8

The water-soluble tetrazolium salt (WST-8) assay was performed according to published methods.[1,3,23] Briefly, 2.5×10^3 ARPE-19/HPV-16 cells per well that had been transfected with the indicated amount of siRNA were seeded into 96-well plates. The following day, the cells were incubated with the indicated concentrations of H_2O_2 or HCA (see Fig. 6). For H_2O_2, cells were treated with H_2O_2 in the serum-free medium for 40 minutes, and subsequently the medium was changed to a normal culture medium. After 72 hours, surviving cells were stained (TetraColor ONE;

Seikagaku Corp., Tokyo, Japan) for 90 minutes at 37°C. The absorbance was then measured at 450 nm.

Cell Viability Analysis

The ARPE-19/HPV-16 cells, that were transfected with the indicated amount of siRNA were seeded into six-well plates at 2.0×10^4 per well. The following day, the cells were incubated with the indicated concentrations of H_2O_2 (see Fig. 6) in serum-free medium for 4 hours, and subsequently the medium was changed to normal culture medium. After 72 hours, the cells were harvested with trypsin. Living cells were counted in a cell viability assay (Adam-MC; NanoEnTek Inc., Seoul, Korea), according to the manufacturer's instructions. Briefly, the cells in each condition were suspended with 100 μL PBS, and each 40 μL was mixed with 40 μL solution T containing propidium iodide (PI) and detergent or 40 μL solution N containing PI without detergent. The number of living cells was calculated as (T number − N number)/T number. The number of living cells without cisplatin was set at 100%.

Statistical Analysis

The Pearson correlation method was used for statistical analysis, and significance was set at the 5% level.

Results

Stress Induction of ATF4

We first investigated endoplasmic reticulum (ER) stress induction of three cell types derived from the eye with TG. ATF4 expression was upregulated by TG treatment in these cell lines. Among these cell lines, ARPE-19/HPV-16 cells showed the highest level of ATF4 expression after treatment with TG (Fig. 1A). In this study, we investigated cellular sensitivity against oxidative stress with the expression of transcription factors, but not physiological properties of retinal pigment epithelium. ARPE-19/HPV-16 cells can be easily maintained and thought to be suitable for our purpose. ARPE-19/HPV-16 cells were then used in the following experiments. We subsequently confirmed the stress induction of ATF4 expression. As shown in Figure 1B, ATF4 expression was upregulated more than threefold after anoxia.

Stress Induction of Nrf2

We previously showed that an E-box was located in the core promoter region of the *ATF4* gene and E-box binding circadian transcriptional factor (clock) positively regulated the *ATF4* gene.[3] We also found one ARE located −300 bp from the transcription start site of the *ATF4* gene promoter. Nrf2 binds to ARE to transactivate the target genes. We investigated whether TG treatment can enhance Nrf2 expression. As shown in Figure 2A, nuclear expression of Nrf2 was increased by TG treatment. Consistent with the result shown in Figure 1A, ARPE-19/HPV-16 cells showed the highest level of Nrf2 expression after treatment with TG. On the other hand, the expression of Keap1, involved in the sequestration of Nrf2, was varied in the cells. Furthermore, Nrf2 expression was induced by anoxia (Fig. 2B). In accordance with the anoxia-dependent induction of Nrf2 expression, Keap1was reduced by anoxia. To investigate whether ATF4 expression requires Nrf2 expression, we performed a knockdown experiment using siRNA for both Nrf2 and Keap1. As shown in Figure 2C, knockdown of Nrf2 expression downregulated ATF4 expression in both transformed (ARPE-19/HPV-16) and nontransformed (HRPEpiC) RPE cells. On the other hand, knockdown of Keap1 upregulated both Nrf2 and ATF4 expression, suggesting that ATF4 is a target gene of Nrf2 (Fig. 2D).

Transcriptional Regulation of the *ATF4* Gene

To confirm the transcriptional expression of the *ATF4* gene, we constructed reporter genes (Fig. 3A). We introduced the

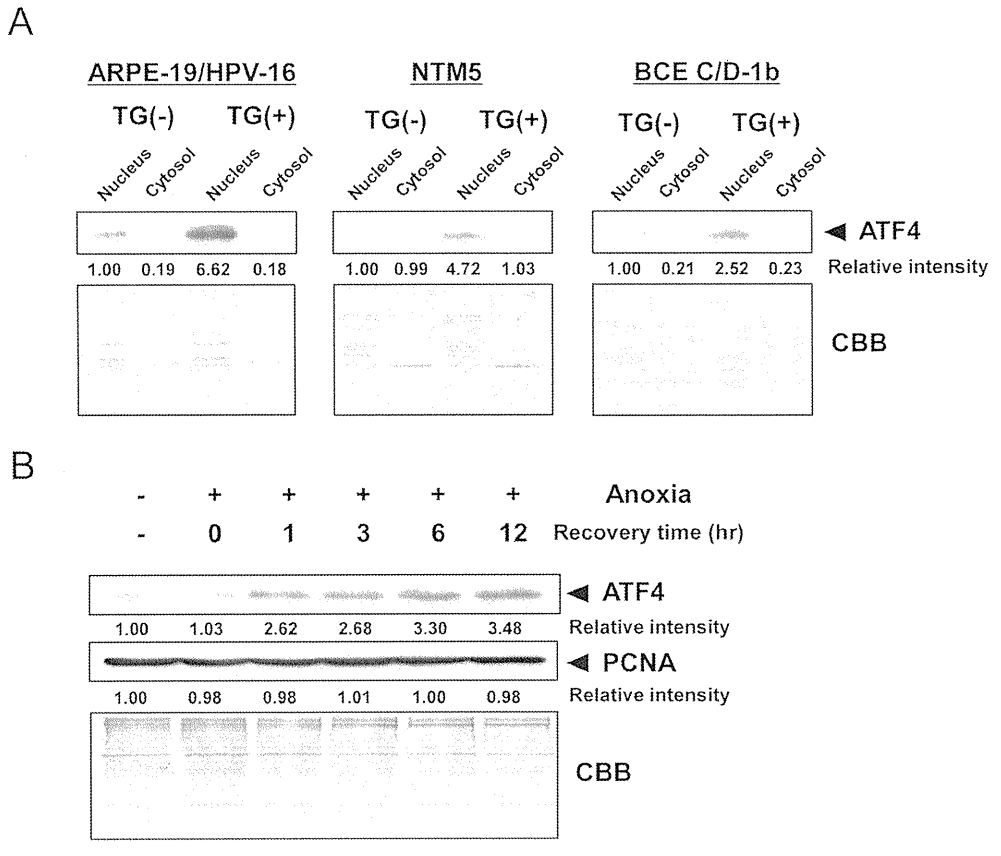

FIGURE 1. (A) The effect of TG on expression of ATF4. ARPE-19/HPV-16 (retina), NTM5 (trabecular meshwork), and BCE C/D-1b (cornea) cells were incubated with or without 1 μM TG for 4 hours. The nuclear and cytosolic extracts containing 50 μg of proteins were prepared and subjected to Western blot analysis with ATF4 antibodies. Relative intensity is shown under each blot. CBB, Coomassie brilliant blue. (B) ATF4 is upregulated in response to anoxic conditions. ARPE-19/HPV-16 cells were incubated in anoxic conditions for 6 hours, and the cells were lysed either immediately or after reoxygenation. The nuclear extracts containing 50 μg of proteins were prepared and subjected to Western blot analysis with the indicated antibodies. Immunoblot analysis of PCNA is shown as a loading control. Relative intensity is shown under each blot.

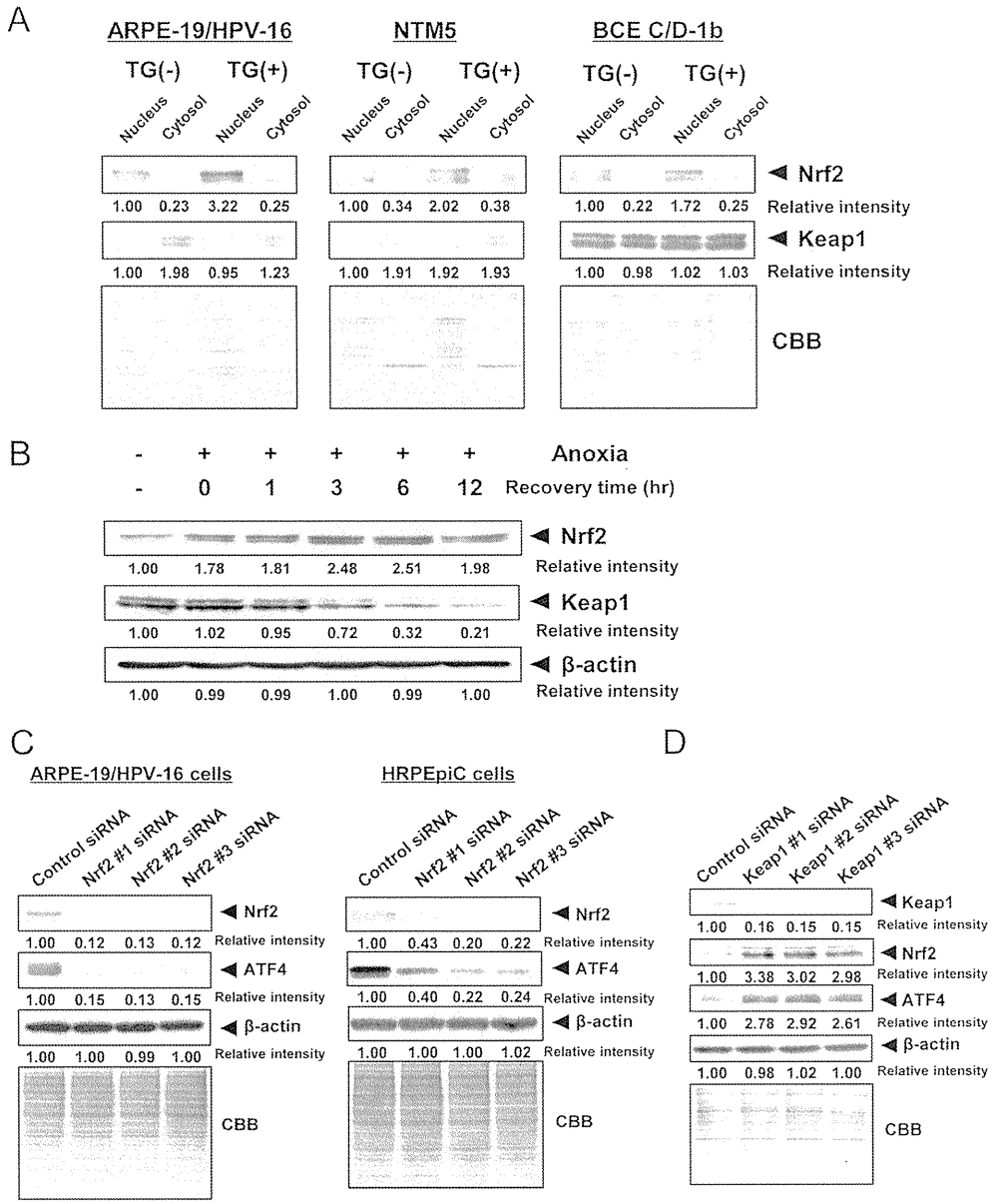

FIGURE 2. (**A**) The effect of TG on expression of Nrf2 expression. ARPE-19/HPV-16, NTM5, corneal endothelial cells were incubated with or without 1 μM TG for 4 hours. Nuclear extracts (100 μg for Nrf2) and cytosolic extracts (50 μg for Keap1) were subjected to SDS-PAGE, and Western blot analysis was performed using the indicated antibodies. Relative intensity is shown under each blot. (**B**) Nrf2 is upregulated in response to anoxic conditions. ARPE-19/HPV-16 cells were incubated in anoxic conditions for 6 hours, and cells were lysed either immediately or after reoxygenation. Nuclear extracts (100 μg for Nrf2) and cytosolic extracts (50 μg for Keap1) were prepared and subjected to Western blot analysis with the indicated antibodies. Immunoblot analysis of β-actin is shown as a loading control. Relative intensity is shown under each blot. (**C**) Nrf2 expression is involved in *ATF4* gene expression in transformed RPE (ARPE-19/HPV-16) cells (*left*) and nontransformed RPE (HRPEpiC) cells (*right*). Control siRNA (100 picomoles) or *Nrf2* siRNA-1, -2, and -3 (100 picomoles) were transfected into indicated cells. The nuclear extracts containing 100 μg of proteins were subjected to SDS-PAGE. The transfer membrane was blotted with indicated antibodies. Immunoblot analysis of β-actin is shown as a loading control. Relative intensity is shown under each blot. (**D**) Keap1 expression is involved in Nrf2 and *ATF4* gene expression. Control siRNA (100 picomoles) or *Keap1* siRNA-1, -2, and -3 (100 picomoles) were transfected into ARPE-19/HPV-16 cells. Nuclear extracts (100 μg for Nrf2 and ATF4) and cytosolic extracts (50 μg for Keap1 and β-actin) were subjected to SDS-PAGE. Transferred membrane was blotted with the indicated antibodies. Immunoblot analysis of β-actin is shown as a loading control. Relative intensity is shown under each blot. CBB, Coomassie brilliant blue.

mutation into ARE. We also constructed the reporter with either a short or long 5′ UTR to test the role of 5′UTR. The promoter activity of the *ATF4* gene was enhanced by co-transfection with the Nrf2 expression plasmid (Fig. 3B). Interestingly, the promoter activity of the *ATF4* gene with short 5′UTR was strongly transactivated by the co-transfection with the Nrf2 expression plasmid. However, Nrf2-dependent transactivation of the ATF4 promoter was completely abolished

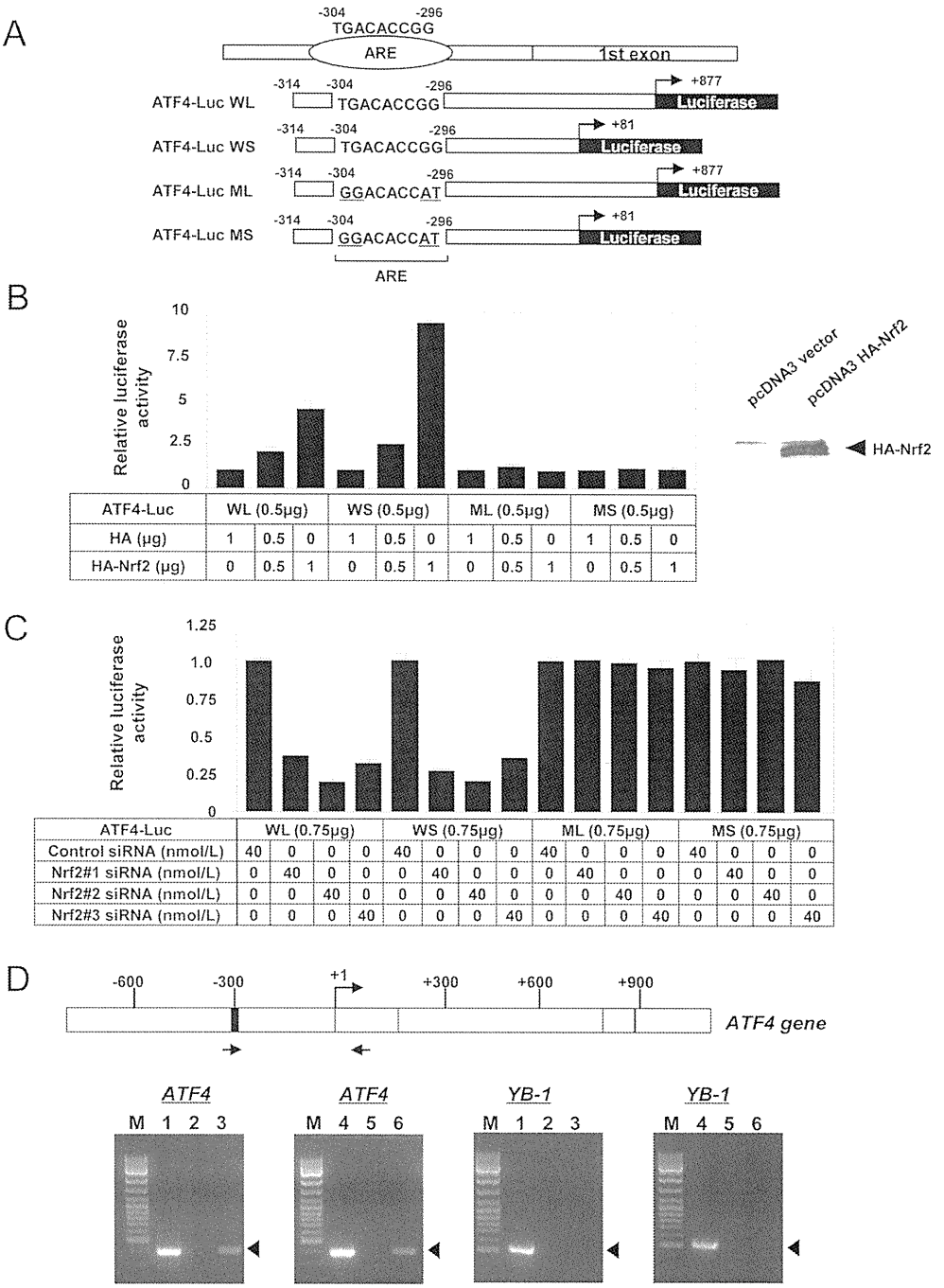

FIGURE 3. (**A**) Representations of *ATF4*-Luc WS, WL, MS, and ML are shown. The reporter plasmids containing wild-type ARE with long or short UTR indicate WL and WS, respectively. The reporter plasmids containing the mutant type of ARE with long or short UTR indicate ML and MS, respectively. (**B**) *Left*: Nrf2 transactivates the promoter activity of the *ATF4* gene. Indicated amounts of *Nrf2* expression plasmid was transiently co-transfected with the indicated reporter plasmids into ARPE-19/HPV-16 cells. The results were normalized to the protein concentration measured using the Bradford method. All values are representative of at least three independent experiments. The luciferase activity of each *ATF4*-Luc with transfection of HA vector corresponds to 1. Bars, SD. *Right*: HA-Nrf2 expression of ARPE-19/HPV-16 cells was detected by Western blot analysis with anti-HA-antibody. (**C**) Knockdown of Nrf2 downregulates the promoter activity of the *ATF4* gene. ARPE-19/HPV-16 cells were transiently transfected with the indicated amounts of control siRNA or *Nrf2* siRNAs followed by transfection with 0.75 μg of the indicated reporter plasmids at intervals of 12 hours. The results shown are normalized to protein concentrations measured using the Bradford method and are representative of at least three independent experiments. The luciferase activity of each *ATF4*-Luc with transfection of control siRNA corresponds to 1. Bars, SD. (**D**) *Top*: Schematic representations of the promoter region and 5′ end of *ATF4* gene. *Arrow*, *black box*, and *gray boxes*: primer, ARE, and exon, respectively. *Bottom*: The ChIP assay was performed with ARPE-19/HPV16 cells. Soluble chromatin (*lanes 1* and *4*) and immunoprecipitated DNAs (*lanes 2* and 5; normal rabbit IgG, *lane 3*; anti-Nrf2 antibody (sc-722), and *lane 6*; anti-Nrf2 antibody RB10471P) were amplified by polymerase chain reaction with specific primer pairs for the ATF4 promoter. *Lane M*: DNA size marker; *arrowhead*: PCR products (389 bp for Nrf2 and 528 bp for YB-1-5).

when the mutation was introduced into ARE. Downregulation of Nrf2 expression also reduced the basal promoter activity of the *ATF4* gene (Fig. 3C). To determine whether transcriptional activation of *ATF4* gene was a result of direct recruitment of Nrf2 to the promoter in vivo, we performed ChIP assays using two different anti-Nrf2 antibodies. ChIP assays demonstrated that Nrf2 bound to the promoter of the *ATF4* gene but not to that of the unrelated YBX1 gene (Fig. 3D).[24]

Role of Nrf2 in Stress Induction of ATF4

Next, we performed reporter assays under oxidative stress. The expression of both Nrf2 and ATF4 was enhanced reproducibly by anoxia. However, ATF4 induction by anoxia was almost cancelled when Nrf2 was downregulated (Fig. 4A). Similar results were also observed when the cells were treated with TG (Fig. 4B). Next, we performed reporter assays under oxidative stress. The assays showed that the promoter activity with wild-type ARE was significantly increased when the cells were treated with H_2O_2 and anoxia (Fig. 5A). Interestingly, the luciferase activity was also enhanced by treatment with H_2O_2 and anoxia, even when reporter constructs containing a long 5′UTR were used. Furthermore, luciferase activity with a long 5′UTR was much higher than that with short a 5′UTR. The stress induction of promoter activity was completely abolished when reporter constructs containing ARE mutations and a short 5′UTR were used. Similar results were observed when the cells were treated with both an ER stress inducer, TG, and an oxidative inducer, HCA (Fig. 5B).

Role of ATF4 Expression in Cellular Sensitivity against Oxidative Stress

ARPE-19/HPV-16 cells were modestly sensitive to H_2O_2 when ATF4 expression was downregulated (Fig. 6A). HCA is thought to induce oxidative stress. Our results showed that the expression of both Nrf2 and ATF4 was induced by HCA treatment (Fig. 6B). The cells were sensitive to HCA even without knockdown of ATF4 expression. There was simply a slight increase in HCA sensitivity after the knockdown of ATF4. To confirm these results, we used an alternative cell viability assay (Adam-MC; NanoEnTek Inc.). The WST-8 measures only the activity of dehydrogenase enzymes derived from living cells (Figs. 6A,

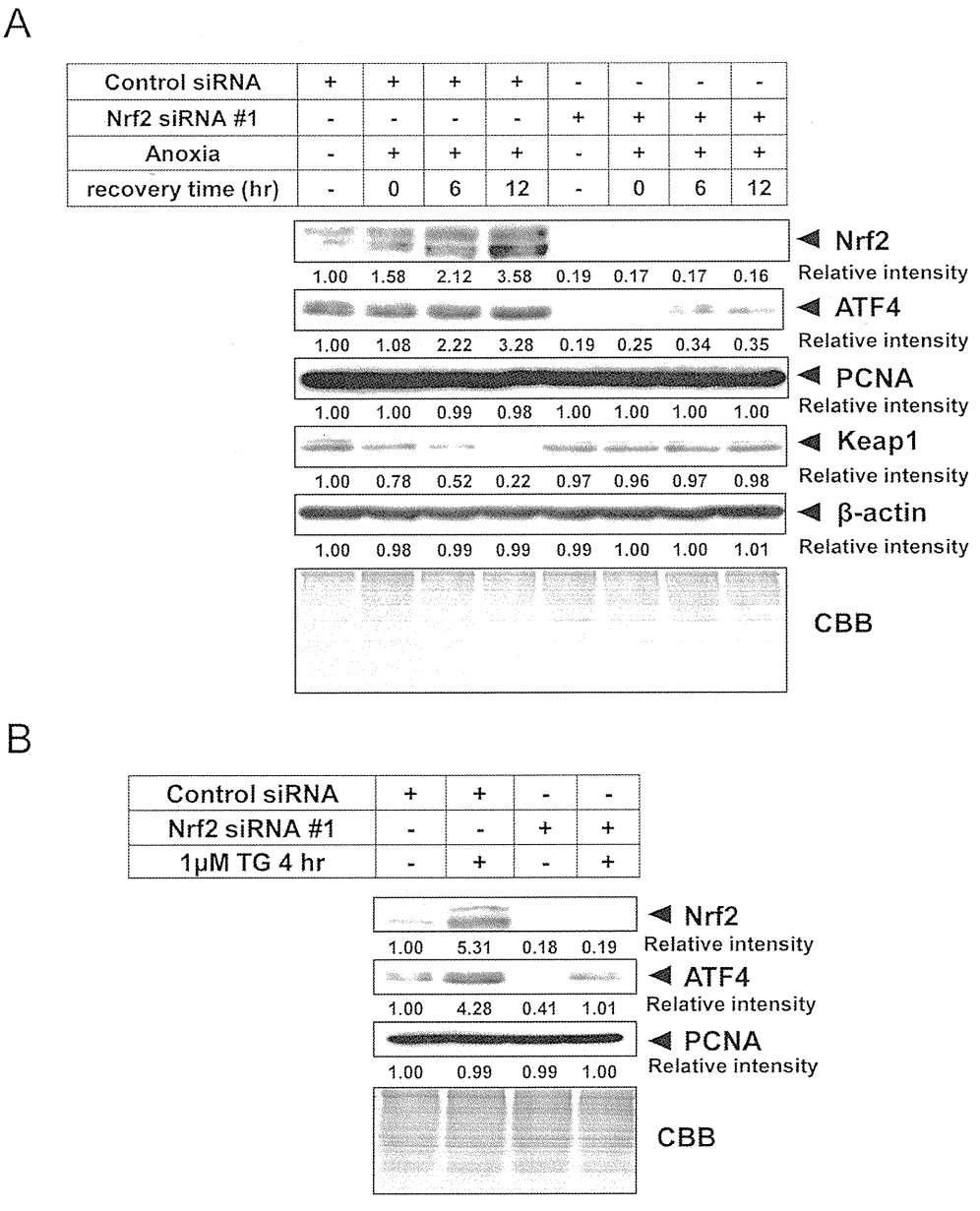

FIGURE 4. Nrf2 regulated the expression of ATF4 under anoxic conditions and ER stress. (**A**) ARPE-19/HPV-16 cells were transiently transfected with 100 picomoles of control siRNA or *Nrf2* siRNA-1. After 48 hours, the cells were incubated in anoxic conditions for 6 hours and were cultured for the indicated recovery times in normal conditions. Nuclear extracts (100 μg for Nrf2, ATF4, and PCNA) and cytosolic extracts (50 μg for Keap1 and β-actin) were subjected to SDS-PAGE. Transferred membrane was blotted with indicated antibodies. PCNA is a loading control for the nuclear fraction, and β-actin is a loading control for the cytosolic fraction. Relative intensity is shown under each blot. (**B**) ARPE-19/HPV-16 cells were transiently transfected with 100 picomoles of control siRNA or Nrf2 siRNA-1. After 48 hours, the cells were incubated with 1 μM TG for 4 hours, and the cells were lysed. Nuclear extracts (100 μg for Nrf2, ATF4, and PCNA) and cytosolic extracts (50 μg for Keap1 and β-actin) were subjected to SDS-PAGE. Transferred membrane was blotted with indicated antibodies. PCNA was a loading control for nuclear fraction, and β-actin was a loading control for cytosolic fraction. Relative intensity is shown under each blot. CBB, Coomassie brilliant blue.

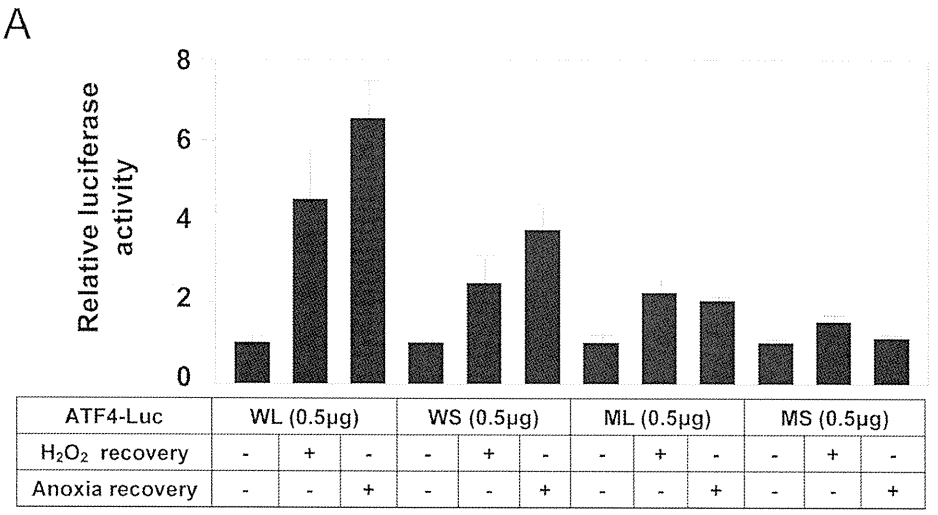

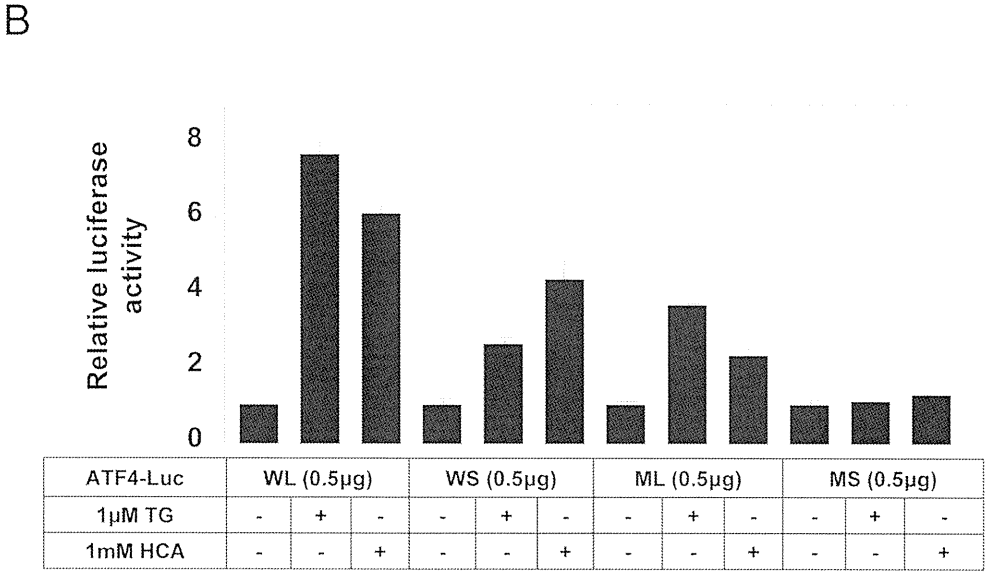

FIGURE 5. The transcriptional activity of ATF4 is upregulated in response to ER stress, oxidative stress, and anoxic conditions. (**A**) ARPE-19/HPV-16 cells were transiently transfected with 0.5 μg *ATF4*-Luc reporter plasmids. At 42 hours after transfection, the cells were incubated at 500 μM H_2O_2 for 2 hours and were further cultured with a new culture medium for 6 hours. At 40 hours after transfection, the cells were cultured in anoxic conditions for 4 hours and were further cultured with a new culture medium and in normal conditions for 4 hours. The results shown are normalized to protein concentrations measured using the Bradford method and are representative of at least three independent experiments. The luciferase activity of each *ATF4*-Luc in normal conditions set to 1. Bars, SD. (**B**) ARPE-19/HPV-16 cells were transiently transfected with 0.5 μg *ATF4*-Luc reporter plasmid. At 36 hours after transfection, the cells were incubated in normal conditions, treated with either 1 μM TG or 1 mM HCA for 6 hours, and subjected to the luciferase assay. The results shown are normalized to protein concentrations measured using the Bradford method and are representative of at least three independent experiments. The luciferase activity of each *ATF4*-Luc under normal conditions set to 1. Bars, SD.

6B). On the other hand, the assay can detect both PI-permeable apoptotic or dead cells and PI nonpermeable living cells. Knockdown of ATF4 expression again rendered the cells sensitive to H_2O_2 (Fig. 6C).

DISCUSSION

Oxidative stressors have been implicated in the pathogenesis of various ocular diseases such as diabetic retinopathy (DR),[25,26] retinopathy of prematurity (ROP),[27,28] age-related macular degeneration (AMD),[29–31] and glaucoma.[32–35] The ability to respond to cellular stressors, including ER and oxidative stress, is fundamentally critical to cellular survival. Cellular stressors can initiate a program of both transcriptional and translational regulation.

We have shown that ATF4 is overexpressed in drug-resistant cells and is involved in glutathione biosynthesis,[3] suggesting that ATF4 expression can protect cells from oxidative stress. We have also shown that the *ATF4* gene is one of the clock-regulated genes indicating that the protective system against oxidative stress may be regulated periodically. In the present study, we showed that activation of both Nrf2 and ATF4 transcription factors coordinates and regulates the convergence of ER and oxidative stress signaling. Furthermore, in addition to translational control, these stressors initiate a transcriptional program for ATF4 expression via Nrf2 activation.

We initially found that ARPE-19/HPV-16 cells derived from retina show a high ATF4 expression in comparison with cells derived from trabecular meshwork and corneal endothelium (Fig. 1A). The retina has the highest metabolic rate and oxygen consumption in the body. The highest metabolic rate and oxygen consumption is usually accompanied by generation of reactive oxygen species. Therefore, the RPE is a primary target of oxidative stress.[36] This finding indicates that an antioxidative system may be highly developed in the RPE to protect the retina. This protective mechanism, via ATF4 activation, is compatible because oxidative stress may occur in infants with retinopathy of prematurity.

Cells respond to various stressors through the upregulation of genes that function specifically to alleviate stress. The activation of these pathways causes increased transcription. On the other hand, translational upregulation of specific mRNA was evident in the ER stress pathway, whereas, ER stress leads to a general inhibition of translation. It has been well studied that ATF4 expression is translationally regulated during conditions of stress.[4–6] However, transcriptional regulation of the *ATF4* gene under oxidative stress remains to be elucidated. Our study clearly showed that constitutive expression of the *ATF4* gene is regulated by Nrf2 (Fig. 2C). Inducible expression

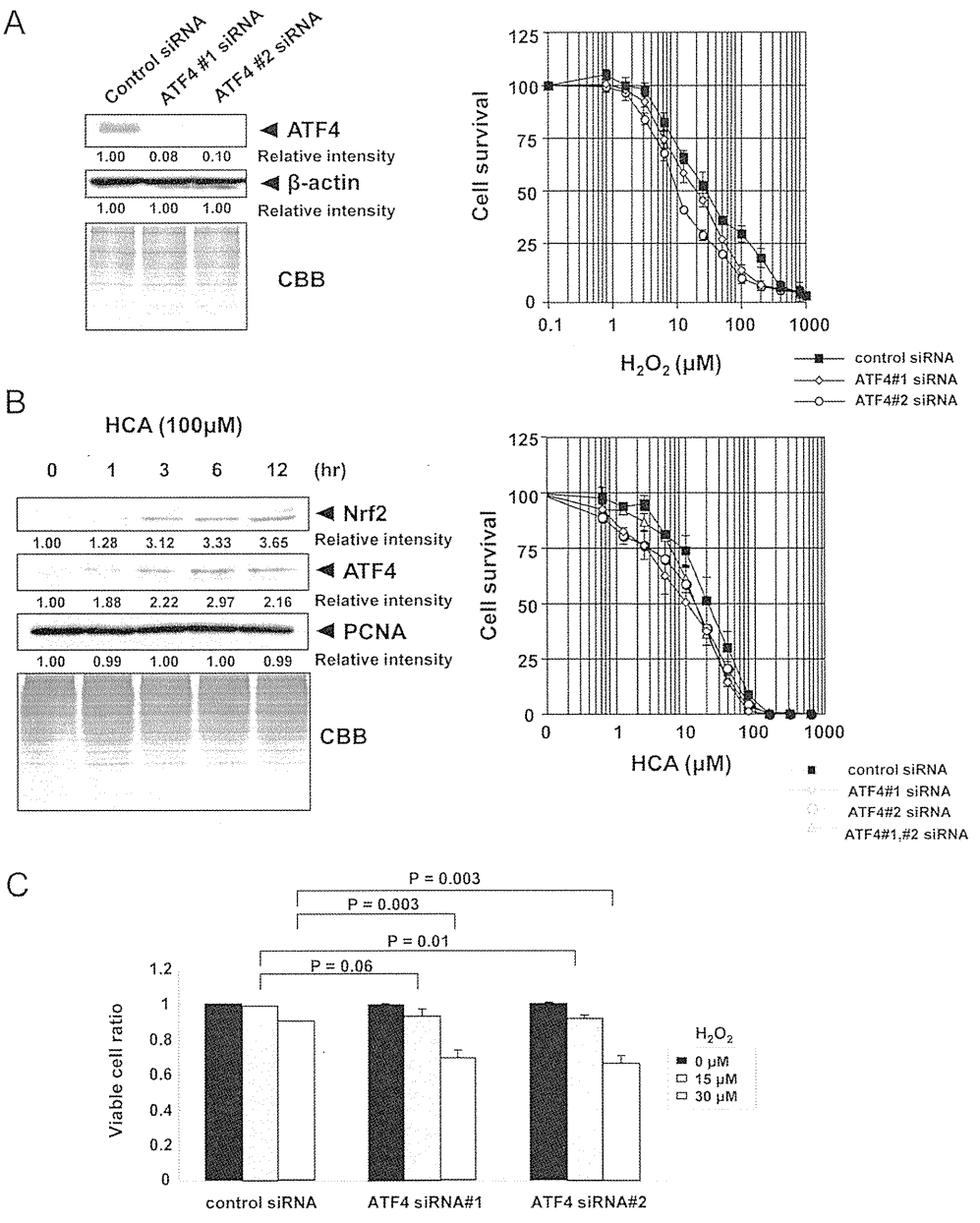

FIGURE 6. (**A**) Downregulation of ATF4 sensitizes ARPE-19/HPV-16 cells to oxidative stress. *Left*: ARPE-19/HPV-16 cells were transiently transfected with 100 picomoles of control, *ATF4* siRNAs. After 72 hours, nuclear extracts (100 μg) were subjected to SDS-PAGE, and Western blot analysis was performed with the indicated antibodies. Immunoblot analysis of β-actin is shown as a loading control. Relative intensity is shown at the bottom of the panel. *Right*: 2.5×10^3 ARPE-19/HPV-16 cells were transfected with 40 nM of control siRNA, ATF4-1 siRNA, and ATF4-2 siRNA. The following day, for induction of oxidative stress, the cells were incubated with the indicated concentrations of H_2O_2 in the serum-free medium for 40 minutes. Then, the medium was replaced with fresh culture medium. After 72 hours, cell survival was analyzed by WST-8 assay. All values are the means of at least three independent experiments. Bars, SD. (**B**) HCA upregulated the expression of Nrf2 and ATF4 in a time-dependent manner. Downregulation of ATF4 sensitized ARPE-19/HPV-16 cells to HCA. *Left*: ARPE-19/HPV-16 cells were incubated with 100 μM HCA for the indicated time. Nuclear extracts (100 μg) were subjected to SDS-PAGE, and Western blot analysis was performed with the indicated antibodies. Immunoblot analysis of PCNA is shown as a loading control. Relative intensity is shown under each blot. *Right*: 2.5×10^3 ARPE-19/HPV-16 cells were transfected with 40 nM of control siRNA, ATF4-1 siRNA, ATF4-2 siRNA. The following day, to induce oxidative stress, cells were incubated with the indicated concentrations of HCA. After 72 hours, cell survival was analyzed by a WST-8 assay. All values are the means of at least three independent experiments. Bars, SD. (**C**) ATF4 is involved in oxidative stress. (**A**) ARPE-19/HPV-16 cells (2.0×10^4 per well) that were transfected with the indicated amount of siRNA were seeded into 6-well plates. The following day, the cells were incubated with the indicated concentrations of H_2O_2. For H_2O_2, the cells were treated with H_2O_2 in the serum-free medium for 4 hours, and subsequently the medium was changed to a normal culture medium. After 72 hours, surviving cells were measured with a cytotoxicity assay. The results with statistical analyses are presented.

of ATF4 under conditions of stress is also upregulated by Nrf2 (Figs. 4A, 4B). In addition to transcriptional regulation, reporter assays suggest that translational regulation of ATF4 expression is present in a 5′UTR-dependent manner (Fig. 5). We also showed that ATF4 expression can protect cells from oxidative stress (Fig. 6). Thus, ATF4 expression is critical to protect cells from oxidative stress. Nrf2 has been shown to regulate target genes through the interaction with ATF4.[17] These data suggest that Nrf2-dependent ATF4 expression may function to augment the expression of Nrf2 target genes via mutual protein–protein interaction. The cellular level of Nrf2 is also regulated by Keap1.[12] Consistent with a previous report,[37] the decrease of Keap1 by anoxia-reoxygenation was also observed, probably due to the increased degradation of Keap1, as shown in Figure 4A. Interestingly, the cellular level of Keap1 during anoxia-reoxygenation was constant when Nrf2 was downregulated, suggesting that the cellular level of Keap1 is regulated by an Nrf2-dependent protein-degradation pathway.

On the other hand, oxidative stress, such as treatment with HCA, increases the expression of vascular endothelial growth factor by an ATF4-dependent mechanism in ARPE-19/HPV-16 cells, suggesting that ATF4 is also involved in angiogenic retinopathy.[38–40] Both arsenite and HCA treatment produce a transient phosphorylation of eIF2α followed by an increase in ATF4 protein levels. This study produced the novel findings that HCA induced the expression of both Nrf2 and ATF4 transcription factors (Fig. 6C). It also showed that downregulation of Keap1 upregulates ATF4 expression (Fig. 2D), indicating that stress induction of ATF4 expression may be regulated mainly by the activation of Nrf2. Consistent with our results, it has been recently shown that Nrf2 is a positive regulator of ATF4.[41]

In summary, the results of our study indicate that ATF4 is transcriptionally regulated under oxidative stress and may be a double-edged sword in the pathogenesis of various retinopathies. Further studies are needed to investigate ATF4 target

gene expression in eye tissues under various types of ER and oxidative stress.

References

1. Miyamoto N, Izumi H, Miyamoto R, et al. Nipradilol and timolol induce Foxo3a and peroxiredoxin 2 expression and protect trabecular meshwork cells from oxidative stress. *Invest Ophthalmol Vis Sci.* 2009;50:2777–2784.
2. Tanabe M, Izumi H, Ise T, et al. Activating transcription factor 4 increases the cisplatin resistance of human cancer cell lines. *Cancer Res.* 2003;63:8592–8595.
3. Igarashi T, Izumi H, Uchiumi T, et al. Clock and ATF4 transcription system regulates drug resistance in human cancer cell lines. *Oncogene.* 2007;26:4749–4760.
4. Rutkowski DT, Kaufman RJ. All roads lead to ATF4. *Dev Cell.* 2003;4:442–444.
5. Blais JD, Filipenko V, Bi M, et al. Activating transcription factor 4 is translationally regulated by hypoxic stress. *Mol Cell Biol.* 2004; 24:7469–7482.
6. Liu L, Wise DR, Diehl JA, Simon MC. Hypoxic reactive oxygen species regulate the integrated stress response and cell survival. *J Biol Chem.* 2008;283:31153–31162.
7. Koumenis C, Naczki C, Koritzinsky M, et al. Regulation of protein synthesis by hypoxia via activation of the endoplasmic reticulum kinase PERK and phosphorylation of the translation initiation factor eIF2α. *Mol Cell Biol.* 2002;22:7405–7416.
8. Koritzinsky M, Magagnin MG, Van den Beucken T, et al. Gene expression during acute and prolonged hypoxia is regulated by distinct mechanisms of translational control. *EMBO J.* 2006;25: 1114–1125.
9. Liu L, Cash TP, Jones RG, Keith B, Thompson CB, Simon MC. Hypoxia-induced energy stress regulates mRNA translation and cell growth. *Mol Cell.* 2006;21:521–531.
10. Fels DR, Ye J, Segan AT, et al. Preferential cytotoxicity of bortezomib toward hypoxic tumor cells via overactivation of endoplasmic reticulum stress pathway. *Cancer Res.* 2008;68:9323–9330.
11. Harding HP, Zhang Y, Zeng H, et al. An integrated stress response regulates amino acid metabolism and resistance to oxidative stress. *Mol Cell.* 2003;11:619–633.
12. Ohta T, Iijima K, Miyamoto M, et al. Loss of keap1 function activates Nrf2 and provides advantages for lung cancer cell growth. *Cancer Res.* 2008;68:1303–1309.
13. Li CQ, Kim MY, Godoy LC, Thiantanawat A, Trudel LJ, Wogan GN. Nitric oxide activation of Keap1/Nrf2 signaling in human colon carcinoma cells. *Proc Natl Acad Sci USA.* 2009;106:14547–14551.
14. Nguyen T, Nioi P, Pickett CB. The Nrf2-antioxidant response element signaling pathway and its activation by oxidative stress. *J Biol Chem.* 2009;284:13291–13295.
15. Chen W, Sun Z, Wang XJ, et al. Direct interaction between Nrf2 and $p21^{Cip1/WAF1}$ upregulates the Nrf2-mediated antioxidant response. *Mol Cell.* 2009;34:663–673.
16. Kaspar JW, Niture SK, Jaiswal AK. Nrf2:INrf2(Keap1) signaling in oxidative stress. *Free Radical Biol Med.* 2009;47:1304–1309.
17. He CH, Gong P, Hu B, et al. Identification of activating transcription factor 4 (ATF4) as an Nrf2-interacting protein. Implication for heme oxygenase-1 gene regulation. *J Biol Chem.* 2001;276:20858–20865.
18. Cullinan SB, Diehl JA. Coordination of ER and oxidative stress signaling: the PERK/Nrf2 signaling pathway. *Int J Biochem Cell Biol.* 2006;38:317–332.
19. Ogawa Y, Saito Y, Nishio K, et al. Gamma-tocopheryl quinone, not alpha-tocopheryl quinone, induces adaptive response through up-regulation of cellular glutathione and cysteine availability via activation of ATF4. *Free Radic Res.* 2008;42:674–687.
20. Oshikawa M, Usami R, Kato S. Characterization of the arylsulfatase I (ARSI) gene preferentially expressed in the human retinal pigment epithelium cell line ARPE-19. *Mol Vis.* 2009;15:482–494.
21. Munderloh UG, Lynch MJ, Herron MJ, et al. Infection of endothelial cells with Anaplasma marginale and A. phagocytophilum. *Vet Microbiol.* 2004;101:53–64.
22. Pang IH, Shade DL, Clark AF, Steely HT, DeSantis L. Preliminary characterization of a transformed cell strain derived from human trabecular meshwork. *Curr Eye Res.* 1994;13:51–63.
23. Miyamoto N, Izumi H, Noguchi T, et al. Tip60 is regulated by circadian transcription factor Clock and is involved in cisplatin resistance. *J Biol Chem.* 2008;26:18218–18226.
24. Shiota M, Izumi H, Onitsuka T, et al. Twist promotes tumor cell growth through YB-1 expression. *Cancer Res.* 2008;68:98–105.
25. Leal EC, Aveleira CA, Castilho AF, et al. High glucose and oxidative/nitrosative stress conditions induce apoptosis in retinal endothelial cells by a caspase-independent pathway. *Exp Eye Res.* 2009; 88:983–991.
26. Kowluru RA, Kanwar M. Oxidative stress and the development of diabetic retinopathy : contributory role of matrix metalloproteinase-2. *Free Radic Biol Med.* 2009;46:1677–1685.
27. Saito Y, Geisen P, Uppal A, Hartnett ME. Inhibition of NAD(P)H oxidase reduces apoptosis and avascular retina in an animal model of retinopathy of prematurity. *Mol Vis.* 2007;13:840–853.
28. Saito Y, Uppal A, Byfield G, Budd S, Hartnett ME. Activated NAD(P)H oxidase from supplemental oxygen induces neovascularization independent of VEGF in retinopathy of prematurity model. *Invest Ophthalmol Vis Sci.* 2008;49:1591–1598.
29. Yang P, Peairs JJ, Tano R, Jaffe GJ. Oxidant-mediated AKT activation in human RPE cells. *Invest Ophthalmol Vis Sci.* 2006;47: 4598–4606.
30. Kim JH, Kim JH, Jun HO, et al. Clusterin protects human pigment epithelial cells from oxidative stress-induced apoptosis. *Invest Ophthalmol Vis Sci.* 2010;51:561–566.
31. Cano M, Thimmalappula R, Fujihara M, et al. Cigarette smoking, oxidative stress, the anti-oxidant response through Nrf2 signaling, and age-related macular degeneration. *Vision Res.* 2010;50:652–664.
32. Maher P, Hanneken A. The molecular basis of oxidative stress-induced cell death in an immortalized retinal ganglion cell line. *Invest Ophthalmol Vis Sci.* 2005;46:749–757.
33. Izzotti A, Bagnis A, Sacca SC. The role of oxidative stress in glaucoma. *Mutat Res.* 2006;612:105–114.
34. Saccà SC, Izzotti A, Rossi P, Traverso C. Glaucomatous outflow pathway and oxidative stress. *Exp Eye Res.* 2007;84:389–399.
35. HE Y, Leung KW, Zhang YH, et al. Mitochondrial complex I defect induces ROS release and degeneration in trabecular meshwork cells of POAG patients: protection by antioxidants. *Invest Ophthalmol Vis Sci.* 2008;49:1447–1458.
36. Fernandes AF, Bian Q, Jiang JK, et al. Proteasome inactivation promotes p38 mitogen-activated protein kinase-dependent phosphatidylinositol 3-kinase activation and increases interleukin-8 production in retinal pigment epithelial cells. *Mol Biol Cell.* 2009;20: 3690–3699.
37. Kim YJ, Ahn JY, Liang P, et al. Human prx1 gene is a target of Nrf2 and is up-regulated by hypoxia/reoxygenation: implication to tumor biology. *Cancer Res.* 2007;67:546–554.
38. Roybal CN, Yang S, Sun CW, et al. Homocysteine increases the expression of vascular endothelial growth factor by a mechanism involving endoplasmic reticulum stress and transcription factor ATF4. *J Biol Chem.* 2004;279:14844–14852.
39. Roybal CN, Hunsaker LA, Barbash O, Vander Jagt DL, Abcouwer SF. The oxidative stressor arsenite activates vascular endothelial growth factor mRNA transcription by an ATF4-dependent mechanism. *J Biol Chem.* 2005;280:20331–20339.
40. Lee I, Lee H, Kim JM, et al. Short-term hyperhomocysteinemia-induced oxidative stress activates retinal glial cells and increases vascular endothelial growth factor expression in rat retina. *Biosci Biotechnol Biochem.* 2007;71:1203–1210.
41. Afonyushkin T, Oskolkova OV, Philippova M, et al. Oxidized phospholipids regulate expression of ATF4 and VEGF in endothelial cells via NRF2-dependent mechanism: novel point of convergence between electrophilic and unfolded protein stress pathways. *Arterioscler Thromb Vasc Biol.* 2010;30:1007–1013.

Journal of Human Genetics (2011) 56, 484–490

www.nature.com/jhg

ORIGINAL ARTICLE

Novel *USH2A* mutations in Japanese Usher syndrome type 2 patients: marked differences in the mutation spectrum between the Japanese and other populations

Hiroshi Nakanishi[1,2], Masafumi Ohtsubo[2], Satoshi Iwasaki[3], Yoshihiro Hotta[4], Shin-ichi Usami[5], Kunihiro Mizuta[1], Hiroyuki Mineta[1] and Shinsei Minoshima[2]

Usher syndrome (USH) is an autosomal recessive disorder characterized by retinitis pigmentosa and hearing loss. USH type 2 (USH2) is the most common type of USH and is frequently caused by mutations in *USH2A*. In a recent mutation screening of *USH2A* in Japanese USH2 patients, we identified 11 novel mutations in 10 patients and found the possible frequent mutation c.8559-2A>G in 4 of 10 patients. To obtain a more precise mutation spectrum, we analyzed further nine Japanese patients in this study. We identified nine mutations, of which eight were novel. This result indicates that the mutation spectrum for *USH2A* among Japanese patients largely differs from Caucasian, Jewish and Palestinian patients. Meanwhile, we did not find the c.8559-2A>G in this study. Haplotype analysis of the c.8559-2G (mutated) alleles using 23 single nucleotide polymorphisms surrounding the mutation revealed an identical haplotype pattern of at least 635 kb in length, strongly suggesting that the mutation originated from a common ancestor. The fact that all patients carrying c.8559-2A>G came from western Japan suggests that the mutation is mainly distributed in that area; indeed, most of the patients involved in this study came from eastern Japan, which contributed to the absence of c.8559-2A>G.
Journal of Human Genetics (2011) **56**, 484–490; doi:10.1038/jhg.2011.45; published online 19 May 2011

Keywords: haplotype; hearing loss; retinitis pigmentosa; Usher syndrome; *USH2A*

INTRODUCTION

Usher syndrome (USH) is an autosomal recessive disorder characterized by retinitis pigmentosa (RP) and hearing loss (HL), with or without vestibular dysfunction.[1] It is the most common cause of combined deafness and blindness in industrialized countries, with a general prevalence of 3.5–6.2 per 100 000 live births.[2–7] The syndrome is clinically and genetically heterogeneous and can be classified into three clinical subtypes on the basis of the severity and progression of HL and the presence or absence of vestibular dysfunction.[8–10]

USH type 2 (USH2) is characterized by congenital mild-to-severe HL and a normal vestibular response; it is the most common type and accounts for >50% of USH cases.[6] Three causative genes have been identified: Usher syndrome 2A (*USH2A*), G-protein coupled receptor 98 (*GPR98*) and deafness, autosomal recessive 31 (*DFNB31*).[11–14] *USH2A*, which encodes usherin, accounts for 74–90% of USH2 cases.[15–17] Usherin is a large protein comprising many functional domains (Figure 1a).[11,12]

Mutation analysis of *USH2A* for the full-length coding region (exons 1–73) in Caucasian patients has revealed the frequent mutation p.Glu767fs (c.2299delG) in exon 13.[18–21] We recently analyzed *USH2A* in Japanese USH2 patients, in which the p.Glu767fs mutation was not identified, and identified 11 novel mutations in 10 patients, indicating that the mutation spectrum of *USH2A* in Japanese patients is considerably different from Caucasians.[22] As 8 of 10 patients had mutations in *USH2A*, the incidence of mutations in the Japanese was similar to that of Caucasians; furthermore, we found the c.8559-2A>G splicing mutation in 4 of 10 patients. We suggested that c.8559-2A>G was a possible frequent *USH2A* mutation among Japanese USH2 patients. In this study, we further performed mutation analysis of *USH2A* in nine USH2 patients to examine if our previous findings were representative of the Japanese population and to obtain a more precise mutation spectrum.

MATERIALS AND METHODS

Subjects and diagnosis

Nine unrelated Japanese patients were referred to Hamamatsu University School of Medicine for genetic diagnosis of USH. All these patients were not related to the previously reported patients[22] and met the following criteria for

[1]Department of Otolaryngology, Hamamatsu University School of Medicine, Hamamatsu, Japan; [2]Department of Photomedical Genomics, Basic Medical Photonics Laboratory, Medical Photonics Research Center, Hamamatsu University School of Medicine, Hamamatsu, Japan; [3]Department of Hearing Implant Sciences, Shinshu University School of Medicine, Matsumoto, Japan; [4]Department of Ophthalmology, Hamamatsu University School of Medicine, Hamamatsu, Japan and [5]Department of Otorhinolaryngology, Shinshu University School of Medicine, Matsumoto, Japan
Correspondence: Dr S Minoshima, Department of Photomedical Genomics, Basic Medical Photonics Laboratory, Medical Photonics Research Center, Hamamatsu University School of Medicine, 1-20-1 Handayama, Higashi-ku, Hamamatsu 431-3192, Japan.
E-mail: mino@hama-med.ac.jp
Received 1 February 2011; revised 30 March 2011; accepted 1 April 2011; published online 19 May 2011

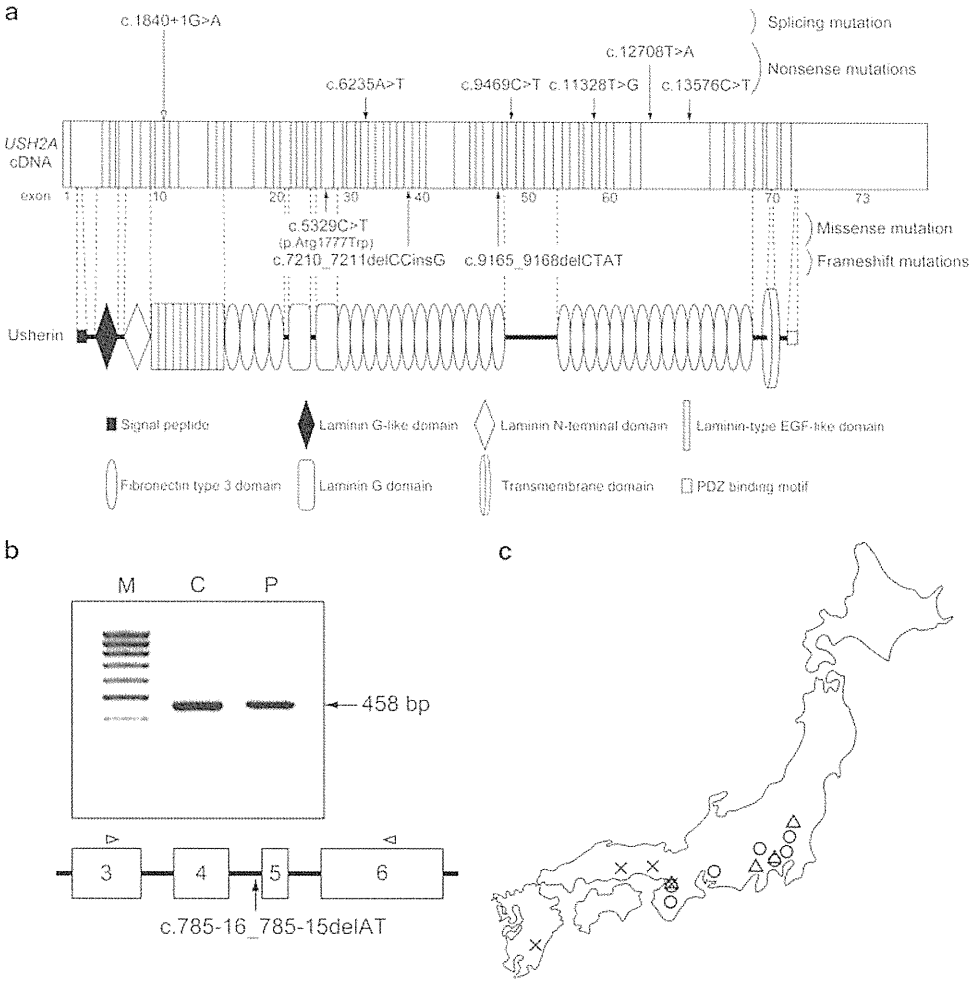

Figure 1 (**a**) Schematic distribution of mutations identified in *USH2A*. Upper, *USH2A* complementary DNA (cDNA) with exon boundaries. Lower, usherin domains encoded by *USH2A*. All mutations were widely distributed almost throughout the entire *USH2A* region without any apparent hot spot. The open arrow indicates a mutation in an intron and closed arrows indicate mutations in exons. (**b**) Products of RT-PCR performed using primers to amplify *USH2A* cDNA between exons 3 and 6. Agarose gel electrophoresis of the RT-PCR products revealed a single band of the size predicted from the normal sequence, indicating that the nucleotide change (c.785-16_785-15delAT) had no effect on splicing and was presumably non-pathogenic. PCR was performed using 2 μg cDNA (total volume, 20 μl) with 40 cycles. The boxes with a number represent exons. The distance between the exons does not indicate the accurate sizes of the introns. The open arrowheads indicate the PCR primers and the arrow indicates the nucleotide change. M, molecular marker (100-bp ladder); C, control; P, patient. (**c**) Schematic distribution of the patients in whom at least one mutated allele was detected. Circles indicate patients included in this study, and triangles and crosses indicate patients included in the previous study. In particular, crosses indicate the patients in whom c.8559-2A>G was detected.

USH2: RP, congenital mild-to-severe HL and normal vestibular function.[8] The clinical evaluation of the affected patients consisted of an elicitation of their medical history, and ophthalmological and audiovestibular examinations. The medical history included their place of birth, age at diagnosis of HL, age at onset of night blindness and age at diagnosis of RP. The details of the ophthalmological and audiovestibular examinations were described in a previous report.[23]

A set of 135 control subjects, selected from Japanese individuals with no visual or hearing impairment, was used to access the frequency of nucleotide sequence variations. The Institutional Review Board of Hamamatsu University School of Medicine approved this study, and written informed consent was obtained from all subjects before enrollment.

Mutation analysis

Genomic DNA was extracted from peripheral lymphocytes with standard procedures. All 73 exons of *USH2A* and their flanking sequences were amplified by PCR. The PCR products were purified with the Wizard SV Gel and PCR Clean-up System (Promega, Madison, WI, USA) or treated with Exonuclease I and Antarctic Phosphatase (New England Biolabs, Ipswich, MA, USA). Direct sequencing was performed using the BigDye Terminator version 3.1 Cycle Sequencing Kit on an ABI 3100 Autosequencer (Applied Biosystems, Foster City, CA, USA). The PCR primers used for *USH2A* amplification were described previously.[22] Using direct sequencing or a restriction enzyme-based assay, we tested the Japanese control chromosomes for the novel mutations identified during the mutation analysis.

In silico analysis for the pathogenicity of a missense mutation

We used the Sort Intolerant From Tolerant (SIFT) (http://sift.jcvi.org)[24] and the polymorphism phenotyping (PolyPhen) (http://genetics.bwh.harvard.edu/pph/)[25] programs to analyze the pathogenicity of a missense mutation. The results from SIFT analysis are given by a probability from 0–1, where mutations with a probability <0.05 are predicted to be 'deleterious,' whereas those with a probability $\geqslant 0.05$ are predicted to be 'tolerated.' PolyPhen describes the mutations as 'benign,' 'possibly damaging' or 'probably damaging.' We applied these programs as described by McGee *et al.*[26]

Reverse-transcriptase (RT)-PCR

We previously showed the significant expression of mRNA in hair roots for seven of nine USH-causing genes (including *USH2A*);[27] therefore, we used total RNA extracted from hair roots and performed RT-PCR to examine the effect of a splicing site change on transcript. Novel PCR primers were designed: forward primer, 5′-GCACAGTAAATGGTTTGCAACCTCCAA-′3 located in exon 3; and reverse primer, 5′-AGGATGGGCTTCAGGATTCAACCG-′3 in exon 6. The amplification conditions were as follows: denaturation at 94 °C for 2 min, 40 cycles of 98 °C for 10 s, 60 °C for 30 s and 68 °C for 1 min, and a final extension at 68 °C for 5 min.

Haplotype analysis

Haplotype pattern within the region surrounding position c.8559-2, where the 'frequent' Japanese mutation c.8559-2A>G was found, was analyzed using a set of 23 single nucleotide polymorphisms (SNPs) (10 sites upstream and 13 sites downstream), which were previously described by ourselves or others.[15,18,20,22,28,29] Haplotype analysis was performed by a direct sequencing method.[12,15,22]

RESULTS

Mutation analysis

Mutation analysis of *USH2A* in the nine unrelated Japanese patients revealed nine probable pathogenic mutations in seven patients (Tables 1 and 2; Figure 1a). Of these, eight mutations were novel (Table 2). The p.Arg1777Trp missense mutation was identified in two patients (C552 and C187), whereas the other mutations were detected in one patient each. The mutations were widely distributed almost throughout the entire region of *USH2A*, without any apparent mutation hot spot (Figure 1a). Two mutations (p.Cys4236X and p.Arg4526X) were found in a homozygous state, of which p.Arg4526X could probably be accounted for by consanguinity (Supplementary Figure 1). In four of the seven patients (C696, C112, C644, and C552), two probable pathogenic alleles were identified and confirmed to be on different chromosomes by using parent or sibling samples (Table 1). For patient C187, segregation analysis could not be performed due to the difficulties in collecting samples from family members. Therefore, we could not confirm whether the two mutations (p.Arg1777Trp and p.Pro2404ValfsX9) were located on different chromosomes. In two patients (C185 and C406), only one mutation was identified; the other mutation remained undetected. None of these nine mutations were found in the Japanese control chromosomes (Table 2).

In the nine mutations identified in this study, seven were of the truncated type, whereas two (c.1840+1G>A and p.Arg1777Trp) were not. The c.1840+1G>A splicing mutation was presumed to be pathogenic because the mutation affected the strictly conserved sequences of a splicing donor site and was not found in 270 Japanese control chromosomes. Its precise effect on splicing was not examined as RT-PCR analysis could not be performed due to the difficulties in collecting hair roots from patient C644. The p.Arg1777Trp missense mutation was also presumed to be pathogenic because the mutation was found in two patients (C552 and C187), but not in 270 Japanese control chromosomes. However, Arg1777 in usherin encoded by *USH2A* was not evolutionally conserved compared with that encoded by orthologous genes of various vertebrates. *In silico* analysis for the pathogenicity of this mutation with the SIFT and PolyPhen programs generated a 'tolerated' rating (probability 0.09) by SIFT and a 'possibly damaging' rating by PolyPhen, which did not exclude the small possibility that this mutation is non-pathogenic. Thus, further analysis may be necessary to determine the precise nature of the mutation.

In addition to the probable pathogenic mutations listed in Table 2, 36 sequence alterations were identified (Table 3 and Supplementary Table 1). These alterations were predicted to be non-pathogenic for

Table 1 Clinical information of patients in whom probable pathogenic mutations were identified

Patient	Age	Gender	Mutations[a] Allele 1	Allele 2	Age (years)[b] HL	NB	RP	Visual acuity Right	Left	Visual field	ERG	Fundus of the eye	Cataract	Severity of HL	Caloric test
Homozygotes															
C696	35	F	p.Cys4236X	p.Cys4236X	3	18	20	0.4	0.5	30–80° (III/4e)	Extinguished	Typical RP	None	Moderate	Normal
C112	48	M	p.Arg4526X	p.Arg4526X	13	11	12	0.15	0.3	10° (V/4e)	Extinguished	Typical RP	Both eyes	Severe	Normal
Compound heterozygotes															
C644	47	F	c.1840+1G>A	p.Tyr3776X	6	10	27	0.07	0.06	10° (V/4e)	Extinguished	Typical RP	Left eye	Moderate	Normal
C552	58	F	p.Arg1777Trp	p.Ile3055MetfsX2	10	15	35	0.1	0.15	5° (V/4e)	Extinguished	Typical RP	Both eyes	Moderate	Normal
C187	30	F	p.Arg1777Trp; p.Pro2404ValfsX9		4	14	29	1.2	1.2	20–30° (III/4e)	Extinguished	Typical RP	None	Moderate	NA
Heterozygote[c]															
C185	53	F	p.Gln3157X	Unknown	5	11	35	0.3	0.3	10° (V/4e)	Extinguished	Typical RP	Both eyes	Severe	Normal
C406	37	F	p.Lys2079X; Unknown		6	21	28	0.7	0.7	40–60° with scotomas (III/4e)	Extinguished	Typical RP	None	Mild	Normal

Abbreviations: ERG, electroretinography; HL, hearing loss; NA, data not available; NB, night blindness; RP, retinitis pigmentosa.
[a]Semicolons that connect mutations indicate that mutations could not be assigned to a paternal or maternal allele.
[b]Age at diagnosis of HL, age at onset of NB and age at diagnosis of RP are shown.
[c]For two patients (C185 and C406), the other pathogenic allele remained undetected.

Table 2 Probable pathogenic mutations identified in the Japanese USH2 patients examined in this study

Mutation type	*Nucleotide change*	*Predicted translation effect*	*Exon/intron number*	*Domain*	*Number of alleles*	*Alleles in control chromosomes*	*Reference*
Nonsense	c.6235A>T	p.Lys2079X	Exon 32	FN3	1	0/64	This report
	c.9469C>T	p.Gln3157X	Exon 48		1	0/130	This report
	c.11328T>G	p.Tyr3776X	Exon 58	FN3	1	0/64	[20]
	c.12708T>A	p Cys4236X	Exon 63	FN3	2	0/220	This report
	c.13576C>T	p.Arg4526X	Exon 63		2	0/64	This report
Frameshift	c.7210_7211delCCinsG	p.Pro2404ValfsX9	Exon 38	FN3	1	0/64	This report
	c.9165_9168delCTAT	p.Ile3055MetfsX2	Exon 46	FN3	1	0/64	This report
Splicing	c.1840+1G>A		Intron 10		1	0/270	This report
Missense	c.5329C>T	p.Arg1777Trp	Exon 27	LamG	2	0/270	This report

Abbreviations: FN3, fibronectin type 3 domain; LamG, laminin G domain.

Table 3 Presumed non-pathogenic alterations that have never been reported

Nucleotide change	*Predicted translation effect*	*Exon/intron number*	*Domain*	*Number of alleles*	*Alleles in control chromosomes*
c.785-16_785-15delAT		Intron 4		1	1/270
c.5573-36delC		Intron 27		1	7/130
c.9258+15T>C		Intron 46		2	
c.13847G>T	p.Gly4616Val	Exon 64	FN3	2	
c.14642G>C	p.Ser4881Thr	Exon 67	FN3	2	3/270

Abbreviation: FN3, fibronectin type 3 domain.

various reasons. Many of them have been reported as polymorphisms in previous reports (Supplementary Table 1). One of the two newly identified alterations within the exons (p.Ser4881Thr) was also identified in the control chromosomes. The other alteration, p.Gly4616Val, was also considered benign because the alteration was detected together with probable pathogenic mutations in patient C187. Two of the three intronic alterations that were in or close to a splicing donor site or branch point sequences (c.785-16_785-15delAT and c.5573-36delC) were also identified in the control chromosomes. As c.785-16_785-15delAT was only found in one control chromosome, RT-PCR analysis was performed to examine its precise effect on splicing. Agarose gel electrophoresis of the RT-PCR products revealed a single band of the size predicted from the normal sequence, indicating that the nucleotide change had no effect on splicing and was presumably non-pathogenic (Figure 1b).

Haplotype analysis

The c.8559-2A>G splicing mutation, which we previously reported as a possible frequent Japanese mutation, was not detected in any patients in this study. To characterize the alleles, which harbor c.8559-2A>G, we analyzed the haplotype pattern of 23 SNP sites (listed in Table 4) within the region surrounding the mutation site for the c.8559-2G and c.8559-2A alleles of all patients in whom at least one mutated allele was detected in this and previous reports.

In all four patients with c.8559-2A>G (C152, C452, C557 and C237), the *USH2A* mutations were in the compound heterozygous state, as we previously reported (Supplementary Table 2). Twenty SNPs located from exon 2 to intron 61 showed the exactly same haplotype pattern for the c.8559-2G (mutated) alleles in three patients (C152, C452 and C557, Table 4). In contrast, the c.8559-2A alleles in these three patients as well as other patients without c.8559-2A>G showed considerably different haplotype patterns (Table 5). As for patient C237, two heterozygous SNP sites in introns 52 and 60 could not be assigned to the c.8559-2A or c.8559-2G allele because of difficulties in obtaining family samples. However, all of the other 18 SNP patterns from exon 2 to intron 61 coincided with the c.8559-2G alleles, but not with any of the c.8559-2A alleles.

Clinical findings

All seven patients in whom at least one mutated allele was identified had developed night blindness at 10–21 years old (mean ± s.d., 14 ± 4.1 years) and had been diagnosed with RP by ophthalmologists at 12–35 years old (27 ± 8.2 years, Table 1). In all patients, the visual fields were symmetrically constricted, pigmentary degeneration was typical for RP with peripheral bone-spicule pigmentation and standard combined electroretinography was extinguished. The best-corrected visual acuity ranged from 1.2 to 0.06. Three patients (C112, C552 and C185) reported having cataracts and underwent cataract surgery in both eyes.

The patients were diagnosed with hearing impairment by otorhinolaryngologists at 3–13 years old (6.7 ± 3.5 years, Table 1). All patients had intelligible speech and wore hearing aids, except for patient C406. Tympanometry yielded normal results consistent with the clinical findings of a normal tympanic membrane and middle ear cavity. Audiograms showed bilateral mild-to-severe sensorineural HL with a typical slope toward high frequencies (mean level, 63.6 ± 15.6 dB).

A delay in motor development was not reported, and all patients started walking before they were 18 months old. The caloric test was normal among all the patients on whom the test was performed; the caloric test was not conducted on patient C187 (Table 1). These results indicate that all patients, except for patient C187, had normal vestibular function, although additional evaluations (for example, the rotary chair test) with potentially greater sensitivity for detecting subtle vestibular dysfunction were not performed.

DISCUSSION

We previously described 14 *USH2A* mutations from 10 Japanese USH2 patients, of which 11 were novel.[22] In this study, we identified nine different mutations from nine patients, of which eight were

Table 4 *USH2A* haplotype patterns of c.8559-2G alleles (genotypes of the patients are shown in Supplementary Table 2)

				C152	*C452*	*C557*	*C237*[a]
Nucleotide nomenclature	*Accession number*	*Exon/intron number*	*Distance from the c.8559-2A>G (kb)*	*AL2*	*AL1*	*AL1*	
c.373A>G	rs10779261	Exon 2	544.1	A	A	A*	A
c.504G>A	rs4253963	Exon 3	540.8	G	G	G*	G
c.1419C>T	rs1805050	Exon 8	445.7	C	C*	C*	C
c.1644+34C>A	rs7515253	Intron 9	444	A	A*	A*	A
c.3157+35A>G	rs1324330	Intron 15	339.5	A	A	A*	A
c.3812-8T>G	rs646094	Intron 17	320.7	T	T	T*	T
c.4457G>A	rs1805049	Exon 21	297.5	A	A	A*	A
c.6317T>C	rs6657250	Exon 32	168.6	T*	T	T	T
c.6506T>C	rs10864219	Exon 34	121.2	T*	T*	T*	T
c.7300+43C>T	rs41277206	Intron 38	56.7	C	C	C*	C
c.8559-2A>G		Intron 42		G	G	G	***A***/G
c.8656C>T	rs41277200	Exon 43	0.067	C*	C	C	C
c.9343A>G	rs56032526	Exon 47	39.9	A*	A	A	A
c.9595A>G	rs4129843	Exon 49	64	A*	A	A	A
c.10232A>C	rs10864198	Exon 52	91.1	C	C	C*	C
c.10388-27T>C	rs7518466	Intron 52	94.9	C	C	C*	***T***/C
c.11231+45C>T	rs17025373	Intron 57	118.3	C*	C*	C	C
c.11504C>T	rs11120616	Exon 59	134.7	C	C	C	C
c.11602A>G	rs35309576	Exon 60	136.4	A	A	A	A
c.11711+71A>T	rs6694510	Intron 60	136.6	T	T	T*	***A***/T
c.12066+73A>G	rs78380529	Intorn 61	149.9	A	A*	A	A
c.12612A>G	rs2797235	Exon 63	202.6	G*	***A***	G	G
c.12666A>G	rs2797234	Exon 63	202.6	A	A	A	A
c.13191G>A	rs2009923	Exon 63	203.2	G*	***A***	G	G

Abbreviation: AL, allele.
Nucleotides described in bold italic style denote that they are different from the others.
Asterisks above nucleotides indicate that segregation analysis was performed to determine which of the two nucleotides exist on the c.8559-2G allele.
[a]For patient C237, segregation analysis was not performed because samples from family members were not available.

novel. As one of these mutations had been previously identified in Scandinavian patients,[20] all of the mutations found in this study were different from the 14 mutations we previously identified. In total, we have identified 23 mutations in 15 of 19 patients, of which 19 were novel. Four mutations, which had been identified in non-Japanese populations, did not include p.Glu767fs, the most prevalent mutation in Caucasians that accounts for ~30% of mutated alleles.[18–21] These results indicate that the mutation spectrum for *USH2A* among Japanese patients largely differs from Caucasian, Jewish and Palestinian patients.[12,18–21,26,29–32] In spite of this difference, the frequency of Japanese patients carrying *USH2A* mutations in USH2 (79%) is similar to that of the above-mentioned populations.[18–20,30,32] For these reasons, mutation screening for *USH2A* is a highly sensitive method for diagnosing USH2, but mutation screening for the p.Glu767fs mutations is not effective among Japanese patients.

In this study, we did not identify the c.8559-2A>G splicing mutation, which we previously reported as a possible frequent mutation in Japanese USH2 patients. SNP analysis for the region surrounding c.8559-2 for the c.8559-2G (mutated) and c.8559-2A (non-mutated) alleles was performed on 15 patients. For the c.8559-2G alleles, we identified the same haplotype pattern over a long range from exon 2 to exon 52 (at least 635 kb) in all four c.8559-2A>G patients; however we did not observe such a haplotype pattern for the c.8559-2A alleles. This indicates that the 635-kb region including c.8559-2A>G is in linkage disequilibrium and strongly suggests that the mutation originated from a common ancestor. In three patients, except for patient C237, the common haplotype region was even longer (at least 694 kb from exon 2 to intron 61). It is quite possible that the c.8559-2G allele of patient C237 also has the same haplotype pattern with that of the other three patients from exon 2 to intron 61; however, we could not examine this in this patient. If that is the case, the 694-kb linkage disequilibrium region is common in all of the c.8559-2G alleles in this study.

It may be worth describing that the four c.8559-2A>G patients were born in western Japan. A possible reason why we did not find the splicing mutation in this study may be that the nine patients analyzed in the present study are mostly from eastern Japan (Figure 1c). Even though the number of patients studied was small, these findings may suggest that the mutation is distributed mainly in western Japan. The fact that c.8559-2A>G was also detected in two Chinese patients suggests the possibility that the mutation occurred in an ancient common ancestor.[33] Further analysis is necessary to obtain a more precise mutation spectrum of *USH2A* in the Japanese.

In conclusion, mutation screening of *USH2A* elucidated nine mutations in seven of nine patients, confirming that mutation screening of *USH2A* is effective for the early diagnosis of USH2 and the mutation spectrum of Japanese patients differs from the spectra of various ethnicities, including Caucasian, Jewish and Palestinian. Haplotype analysis of the c.8559-2A>G allele indicated that it originated from an ancestral mutational event and the mutation was likely to be distributed mainly in western Japan. Most of the patients involved in this study came from eastern Japan, which contributed to the absence of c.8559-2A>G in this study. Further analysis is necessary to obtain a more precise mutation spectrum of *USH2A* in the Japanese.

Table 5 ***USH2A*** haplotype patterns of c.8559-2A alleles (Genotypes of the patients are shown in Table 1 and Supplementary Table 2)

Nucleotide	C696		C112		C644		C552		C187[a]	C185	C406[a]	C712		C116		C152[b]	C452[b]	C557[b]	C237[a,b]	C212[a]	C332
nomenclature	AL1	AL2	AL1	AL2	AL1	AL2	AL1	AL2		AL1		AL1	AL2	AL1	AL2	AL1	AL2	AL2			AL1
c.373A>G	***G***	***G***	A	A	A	A	A	A	A	A	A/***G***	A	A	A	***G***	A	A	***G***	A	A	A
c.504G>A	***A***	***A***	G	G	G	G	G	G	G	G	G/***A***	G	G	G	***A***	G	G	***A***	G	G	G
c.1419C>T	C	C	C	C	C	C	C	C	C	C	C/***T***	C	C	C	***T***	C	***T***	***T***	C	C	C
c.1644+34C>A	A	A	A	A	A	A	A	A	A	A	***C***	A	A	A	***C***	A	***C***	***C***	A	A	A
c.3157+35A>G	***G***	***G***	A	A	A	A	A	A	A	A	A/***G***	A	A	A	***G***	A	A	***G***	A	A	A
c.3812-8T>G	T	T	T	T	T	T	T	T	T	T	T/***G***	T	T	T	***G***	T	T	***G***	T	T	T
c.4457G>A	***G***	***G***	A	A	A	A	A	A	A	A	***G***/A	A	A	A	***G***	A	A	***G***	A	A	A
c.6317T>C	T	T	T	T	***C***	***C***	***C***	***C***	T/***C***	***C***	T/***C***	***C***	***C***	T	T	***C***	T	T	T	T/***C***	T
c.6506T>C	***C***	***C***	***C***	***C***	***C***	***C***	***C***	***C***	***C***	***C***	***C***	T	***C***	***C***	***C***	***C***	***C***	***C***	T	***C***	***C***
c.7300+43C>T	C	C	C	C	C	C	C	C	C	C	C	C	C	C	C	C	C	***T***	C	C	C
c.8559-2A>G	***A***	***A***	***A***	***A***	***A***	***A***	***A***	***A***	***A***	***A***	***A***	***A***	***A***	***A***	***A***	***A***	***A***	***A***	***A***/G	***A***	***A***
c.8656C>T	C	C	***T***	***T***	***T***	***T***	C	C	C	***T***	C	C	C	C	C	***T***	C	C	C	C	C
c.9343A>G	A	A	***G***	***G***	A	A	A	A	A	***G***	A/***G***	A	A	A	A	***G***	A	A	A	A	***G***
c.9595A>G	A	A	***G***	***G***	A	A	A	A	A	***G***	A/***G***	A	A	A	A	***G***	A	A	A	A	***G***
c.10232A>C	C	C	C	C	C	C	C	C	C	C	***A***/C	C	C	C	C	C	C	***A***	C	***A***/C	C
c.10388-27T>C	C	C	C	C	C	C	C	C	C	C	***T***/C	C	C	C	C	C	C	***T***	***T***/C	***T***/C	C
c.11231+45C>T	***T***	***T***	***T***	***T***	C	***T***	***T***	C	C/***T***	C	C	C	***T***	***T***	***T***	***T***	***T***	C	C	C/***T***	C
c.11504C>T	C	C	***T***	***T***	***T***	C	C	C	C	C	C	***T***	***T***	C	C	C	C	C	C	C	C
c.11602A>G	A	A	**G**	***G***	***G***	A	A	A	A	A	A/***G***	***G***	A	A	A	A	A	A	A	A	A
c.11711+71A>T	T	T	T	T	T	T	T	***A***	***A***/T	***A***	***A***/T	T	T	T	T	T	T	***A***	***A***/T	***A***/T	***A***
c.12066+73A>G	A	A	A	A	A	A	A	A	A/***G***	A	A	A	A	***G***	***G***	A	***G***	A	A	A	A
c.12612A>G	A	A	A	A	A	G	A/G[c]		A/G	G	A/G	G	G	A	A	A	A	G	G	G	A
c.12666A>G	A	A	A	A	A	A	A	A	A	G	A/G	A	A	A	A	A	A	A	A	A/G	A/G[c]
c.13191G>A	A	A	A	A	A	G	A	G	G/A	G	G/A	G	G	A	A	A	A	G	G	G	A

Abbreviation: AL, allele.
Nucleotides described in bold italic style denotes that they are different from that of c.8559-2G alleles ranging from c.373A>G to c.12066+73A>G shown in Table 4.
[a]For four patients (C187, C406, C237 and C212), segregation analysis was not performed because samples from family members were not available.
[b]For four patients (C152, C452, C557 and C237), the haplotypes for c.8559-2G alleles are shown in Table 4.
[c]For two single nucleotide polymorphisms (c.12612A>G on patient C552 and c.12666A>G on patient C332), genotyping was incomplete because both of the parents also had A/G alleles.

ACKNOWLEDGEMENTS

We thank all the subjects who participated in this study. This work was supported by research grants from the Ministry of Labor and Welfare (Acute Profound Deafness Research Committee) and the Ministry of Education, Culture, Sports, Science, and Technology (Young Scientists Grant B-22791589) in Japan.

1 Yan, D. & Liu, X. Z. Genetics and pathological mechanisms of Usher syndrome. *J. Hum. Genet.* **55,** 327–335 (2010).
2 Nuutila, A. Dystrophia retinae pigmentosa—dysacusis syndrome (DRD): a study of the Usher or Hallgren syndrome. *J. Genet. Hum.* **18,** 57–88 (1970).
3 Boughman, J. A., Vernon, M. & Shaver, K. A. Usher syndrome: definition and estimate of prevalence from two high-risk populations. *J. Chronic Dis.* **36,** 595–603 (1983).
4 Grondahl, J. Estimation of prognosis and prevalence of retinitis pigmentosa and Usher syndrome in Norway. *Clin. Genet.* **31,** 255–264 (1987).
5 Hope, C. I., Bundey, S., Proops, D. & Fielder, A. R. Usher syndrome in the city of Birmingham: prevalence and clinical classification. *Br. J. Ophthalmol.* **81,** 46–53 (1997).
6 Rosenberg, T., Haim, M., Hauch, A- M. & Parving, A. The prevalence of Usher syndrome and other retinal dystrophy-hearing impairment associations. *Clin. Genet.* **51,** 314–321 (1997).
7 Spandau, U. H. & Rohrschneider, K. Prevalence and geographical distribution of Usher syndrome in Germany. *Graefes Arch. Clin. Exp. Ophthalmol.* **240,** 495–498 (2002).
8 Kimberling, W. J. & Möller, C. Clinical and molecular genetics of Usher syndrome. *J. Am. Acad. Audiol.* **6,** 63–72 (1995).
9 Tsilou, E. T., Rubin, B. I., Caruso, R. C., Reed, G. F., Pikus, A., Hejtmancik, J. F. *et al.* Usher syndrome clinical types I and II: could ocular symptoms and signs differentiate between the two types? *Acta. Ophthalmol. Scand.* **80,** 196–201 (2002).
10 Pennings, R. J. E., Huygen, P. L. M., Orten, D. J., Wagenaar, M., van Aarem, A., Kremer, H. *et al.* Evaluation of visual impairment in Usher syndrome 1b and Usher syndrome 2a. *Acta. Ophthalmol. Scand.* **82,** 131–139 (2004).
11 Eudy, J. D., Weston, M. D., Yao, S., Hoover, D. M., Rehm, H. L., Ma-Edmonds, M. *et al.* Mutation of a gene encoding a protein with extracellular matrix motifs in Usher syndrome type IIa. *Science* **280,** 1753–1757 (1998).
12 van Wijk, E., Pennings, R. J., te Brinke, H., Claassen, A., Yntema, H. G., Hoefsloot, L. H. *et al.* Identification of 51 novel exons of the Usher syndrome type 2A (USH2A) gene that encode multiple conserved functional domains and that are mutated in patients with Usher syndrome type II. *Am. J. Hum. Genet.* **74,** 738–744 (2004).
13 Weston, M. D., Luijendijk, M. W., Humphrey, K. D., Moller, C. & Kimberling, W. J. Mutations in the VLGR1 gene implicate G-protein signaling in the pathogenesis of Usher syndrome type II. *Am. J. Hum. Genet.* **74,** 357–366 (2004).
14 Ebermann, I., Scholl, H. P., Charbel Issa, P., Becirovic, E., Lamprecht, J., Jurklies, B. *et al.* A novel gene for Usher syndrome type 2: mutations in the long isoform of whirlin are associated with retinitis pigmentosa and sensorineural hearing loss. *Hum. Genet.* **121,** 203–211 (2007).
15 Weston, M. D., Eudy, J. D., Fujita, S., Yao, S., Usami, S., Cremers, C. *et al.* Genomic structure and identification of novel mutations in usherin, the gene responsible for Usher syndrome type IIa. *Am. J. Hum. Genet.* **66,** 1199–1210 (2000).
16 Dreyer, B., Tranebjaerg, L., Brox, V., Rosenberg, T., Moller, C., Beneyto, M. *et al.* A common ancestral origin of the frequent and widespread 2299delG USH2A mutation. *Am. J. Hum. Genet.* **69,** 228–234 (2001).
17 Pennings, R. J., Te Brinke, H., Weston, M. D., Claassen, A., Orten, D. J., Weekamp, H. *et al.* USH2A mutation analysis in 70 Dutch families with Usher syndrome type II. *Hum. Mutat.* **24,** 185 (2004).
18 Aller, E., Jaijo, T., Beneyto, M., Najera, C., Oltra, S., Ayuso, C. *et al.* Identification of 14 novel mutations in the long isoform of USH2A in Spanish patients with Usher syndrome type II. *J. Med. Genet.* **43,** e55 (2006).
19 Baux, D., Larrieu, L., Blanchet, C., Hamel, C., Ben Salah, S., Vielle, A. *et al.* Molecular and in silico analyses of the full-length isoform of usherin identify new pathogenic alleles in Usher type II patients. *Hum. Mutat.* **28,** 781–789 (2007).
20 Dreyer, B., Brox, V., Tranebjaerg, L., Rosenberg, T., Sadeghi, A. M., Moller, C. *et al.* Spectrum of USH2A mutations in Scandinavian patients with Usher syndrome type II. *Hum. Mutat.* **29,** 451 (2008).